iScience

CellPress
OPEN ACCESS

Article

Matrix stiffness induces epithelial-to-mesenchymal transition via Piezo1-regulated calcium flux in prostate cancer cells

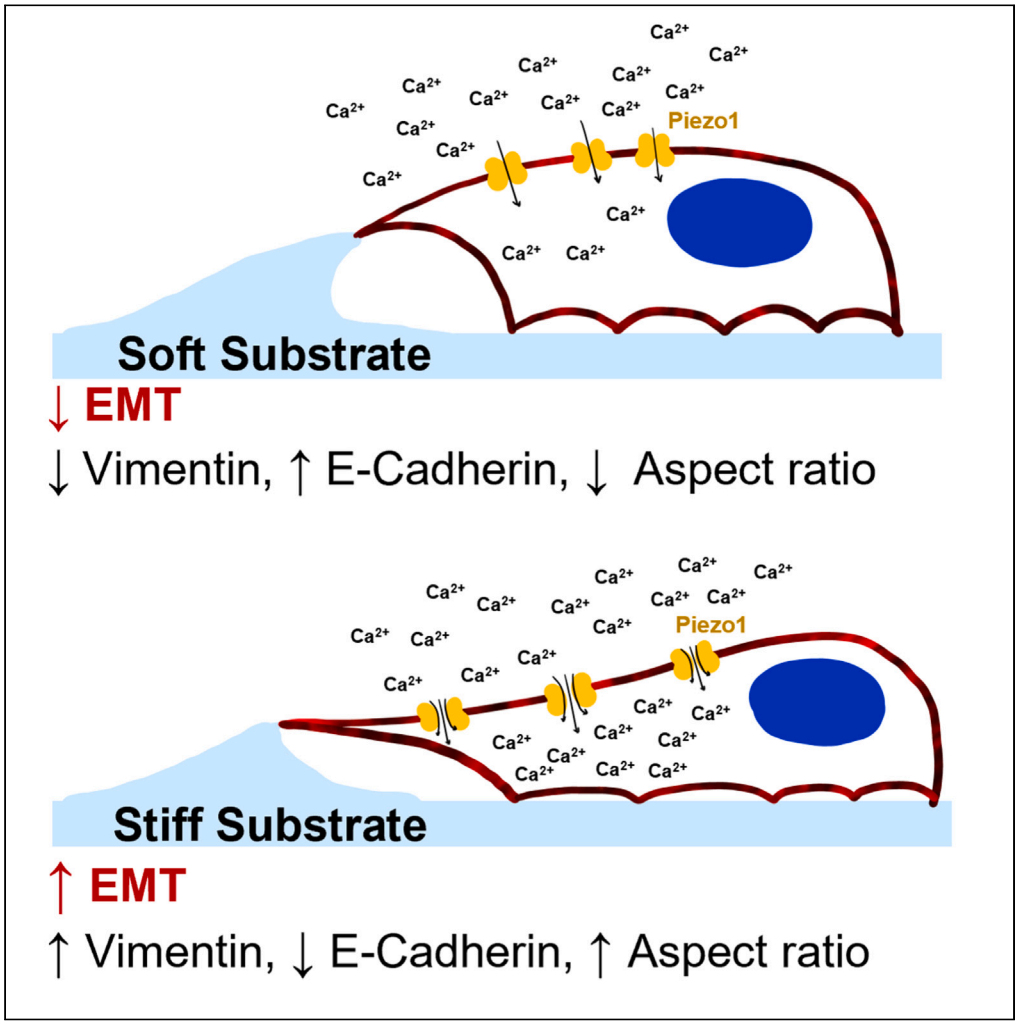

Maria Lopez-Cavestany, Su Bin Hahn, Jacob M. Hope, ..., Jacob A. VanderBurgh, Cynthia A. Reinhart-King, Michael R. King

mike.king@vanderbilt.edu

Highlights

The mechanosensitive ion channel Piezo1 is involved in EMT progression in cancer cells

Increasing substrate stiffness causes intracellular calcium concentrations to rise

Yoda1 increases EMT progression of prostate cancer cells grown on soft substrates

GsMTx-4 inhibits EMT in prostate cancer cells grown on stiff substrates

Lopez-Cavestany et al., iScience 26, 106275
April 21, 2023
https://doi.org/10.1016/j.isci.2023.106275

iScience

CellPress
OPEN ACCESS

Article

Matrix stiffness induces epithelial-to-mesenchymal transition via Piezo1-regulated calcium flux in prostate cancer cells

Maria Lopez-Cavestany,[1] Su Bin Hahn,[1] Jacob M. Hope,[1] Noah T. Reckhorn,[1] Joshua D. Greenlee,[1] Samantha C. Schwager,[1] Jacob A. VanderBurgh,[1] Cynthia A. Reinhart-King,[1] and Michael R. King[1,2,*]

SUMMARY

Cells utilize calcium channels as one of the main signaling mechanisms to sense changes in the extracellular space and convert these changes to intracellular signals. Calcium regulates several key signaling networks, such as the induction of EMT. The current study expands on the understanding of how EMT is controlled via the mechanosensitive calcium channel Piezo1 in cancerous cells, which senses changes in the extracellular matrix stiffness. We model the biophysical environment of healthy and cancerous prostate tissue using polyacrylamide gels of different stiffnesses. Significant increases in calcium steady-state concentration, vimentin expression, and aspect ratio, and decreases in E-cadherin expression were observed by increasing matrix stiffness and also after treatment with Yoda1, a chemical agonist of Piezo1. Overall, this study concludes that Piezo1-regulated calcium flux plays a role in prostate cancer cell metastatic potential by sensing changes in ECM stiffness and modulating EMT markers.

INTRODUCTION

Epithelial-to-mesenchymal transition (EMT) has been associated with tumor progression and cancer cell metastatic potential, enabling cells to escape the primary tumor and extravasate into the bloodstream.[1] It is a combination of morphological and biochemical changes that reduce cell-cell recognition and adhesion, leading to increased motility, invasiveness, and resistance to apoptosis.[2,3] EMT is defined by changes in basement membrane remodeling, activation of differentiation genes, remodeling of the cytoskeleton, downregulation of epithelial proteins that aid in cell-to-cell adhesion (E-cadherin), and the upregulation of mesenchymal proteins such as N-cadherin and vimentin.[1,3,4] EMT is additionally characterized by the acquisition of a mesenchymal cell morphology because of a loss of the apical-basal polarity of epithelial cells. However, EMT does not produce a stable cell state; it is a multidimensional process typically resulting in hybrid cells that fall somewhere on the axis between epithelial and mesenchymal states.[1,4]

There exists a complex array of signals which induce EMT, making it a highly heterogeneous process. These range from biochemical signals, interactions with other cell types such as stromal cells, and changes to the extracellular matrix.[5] Increased extracellular matrix stiffness is known to play a prominent role in EMT and cancer metastasis.[6–9] In prostate cancer, the mean tumor stiffness is 60 kPa as measured with transrectal shear-wave elastography, and ranges from 30 kPa to 110 kPa.[10] Moreover, there is a high degree of intratumoral stiffness heterogeneity.[11,12] In contrast, healthy prostatic tissue has a mean stiffness of 5 kPa, but can range to a maximum stiffness that ranges up to 35 kPa.[13]

As cells migrate through their environment, they exert tensile forces on the substrate.[14] This is counteracted by the viscoelastic properties of their surroundings as the matrix resists deformation. Cancer cells can sense these forces via mechanosensitive ion channels, which convert mechanical cues in the cells' environment to intracellular biochemical signals. Piezo1, discovered by the 2021 Nobel Prize winner for Physiology or Medicine, Dr. Patapoutian, is a mechanosensitive ion channel that regulates calcium flux into cells by opening in direct response to lateral membrane tension and cytoskeletal tethers.[15–18] In the closed/low tension state, Piezo1 stores potential energy for gating through its dome-like structure. When transitioning to the open state, the dome is flattened in proportion to the energy of the system. In this way, Piezo1 channels are gated by changing tension in the cell membrane with high sensitivity, resulting in increased calcium

[1]Department of Biomedical Engineering, Vanderbilt University, Nashville, TN 37235, USA

[2]Lead contact

*Correspondence: mike.king@vanderbilt.edu

https://doi.org/10.1016/j.isci.2023.106275

influx. In addition to sensitivity to forces in the lipid membrane, the Piezo1 channel is known to open and close in reaction to traction forces generated by the cellular cytoskeleton.[19,20]

Under healthy conditions, Piezo1 allows endothelial cells to sense and react to shear forces in the bloodstream which helps to control vascular tone and the baroreceptor reflex.[21] In addition, Piezo1 plays a crucial role in the gastrointestinal tract, urinary tract, joints, lungs, and touch sensation. In prostate cancer, Piezo1 is highly upregulated compared to healthy prostatic tissue.[22] In the study by *Han* et al., it was observed when comparing para-carcinoma and carcinoma tissue samples isolated from a patient, and by comparing the prostate cancer cell lines PC3 and DU145 to the healthy prostate cell line RWPE-1. That study also found that Piezo1 plays a role in colony formation, cell migration, and wound healing *in vitro*. *In vivo*, Piezo1 silencing in a murine subcutaneous model of prostate cancer led to decreased tumor volume and weight in the same study. These results were also confirmed in a *Drosophila* glioma model.[23] Piezo1 was found to be necessary for glioma cell proliferation and tumor stiffening. In addition, *Chen* et al. found that glioma aggressiveness correlated with Piezo1 expression. Overall, this evidence shows that Piezo1 is a key player in promoting cancer progression. In a separate study on prostate cancer, we showed that pharmacologically activating Piezo1 sensitized cells to TRAIL-mediated apoptosis.[24] This parallels the results observed when cancer cells are treated with TRAIL and exposed to physiological levels of fluid shear stress.[25] This further supports the importance of Piezo1 in various mechanisms of prostate cancer progression.

The current study expands on the understanding of how EMT is modulated via Piezo1 sensing of the extracellular matrix stiffness surrounding cancerous cells. Herein, we model the biophysical environment of healthy and cancerous prostate tissue using 5 kPa and 60 kPa polyacrylamide (PA) gels coated with collagen I. Glass coverslips were utilized as a positive control for stiffness conditions. Although substrates this stiff do not directly correspond to with physiological conditions, it enables us to address where the upper bound of increasing calcium concentration and EMT progression because of stiffness is, and how closely cells grown on the PA gels are able to reach this level of activation. We report on the effects of matrix stiffness and the pharmacological inactivation and activation of Piezo1 on EMT-associated changes in the metastatic prostate cancer cell lines PC3 and DU145. PC3 cells represent a highly metastatic cell line and therefore already exhibit an advanced grade of EMT, whereas DU145 are considered a moderately metastatic cell line and begin closer to the epithelial state.[26] Significant changes in calcium steady-state concentration, vimentin expression, and actin polymerization were observed in the high stiffness groups compared to cells on the low stiffness substrates. In addition, these changes were comparable to those observed when both cell lines were grown on soft substrates when treated with Yoda1, a chemical agonist of Piezo1. Overall, this study provides insight highlighting the importance of Piezo1 in cancer cell mechanosensing and metastatic potential in prostate cancer.

RESULTS

Stiffer substrates lead to increased steady-state calcium and EMT-related protein expression

To address previous observations in the literature that increasing stiffness plays a role in intracellular free calcium modulation and is implicated in the progression of the EMT cell phenotype, the prostate cancer cell lines DU145 and PC3 were plated onto substrates of three different stiffnesses. The softest substrate was a PA gel with an elastic modulus of 5 kPa, recapitulating the stiffness the cells would experience in healthy prostatic tissue.[13] The second PA gel modeled the stiffness in an advanced stage prostate tumor which typically has a measured mean stiffness of 60 kPa.[10] The stiffness of both gels was confirmed via AFM (Figure S1). Lastly, glass coverslips were used as a positive control for stiffness because it represents an effectively infinitely stiff environment for the cells, as glass fibers exhibit a Young's modulus of about 72 GPa. The substrates were collagen-coated, and cells were incubated for a total of 72h to allow them to adhere and grow. Intracellular calcium concentrations were observed utilizing the calcium probe Fluo-4. The average fluorescence, or $\Delta F/F_0$, was calculated by subtracting the background noise from the average fluorescent signal of the cells, and then dividing by the background noise.

Steady-state calcium in prostate cancer cells is heavily influenced by the stiffness of the substrate the cells are grown on, as seen in the micrographs in Figure 1A. DU145 cells on the 60 kPa gels and the glass control showed a 29.5% and 47.1% increase in calcium concentration, respectively, compared to cells grown on the softest PA gels (Figure 1B). Steady-state calcium in the PC3 cells showed similar sensitivity to substrate stiffness as the DU145 cells (Figure 1C). PC3 cells on the 60 kPa gels and the glass control showed a 46.5% and 60.6% increase in calcium concentration, respectively, compared to cells grown on the softest PA gels. The

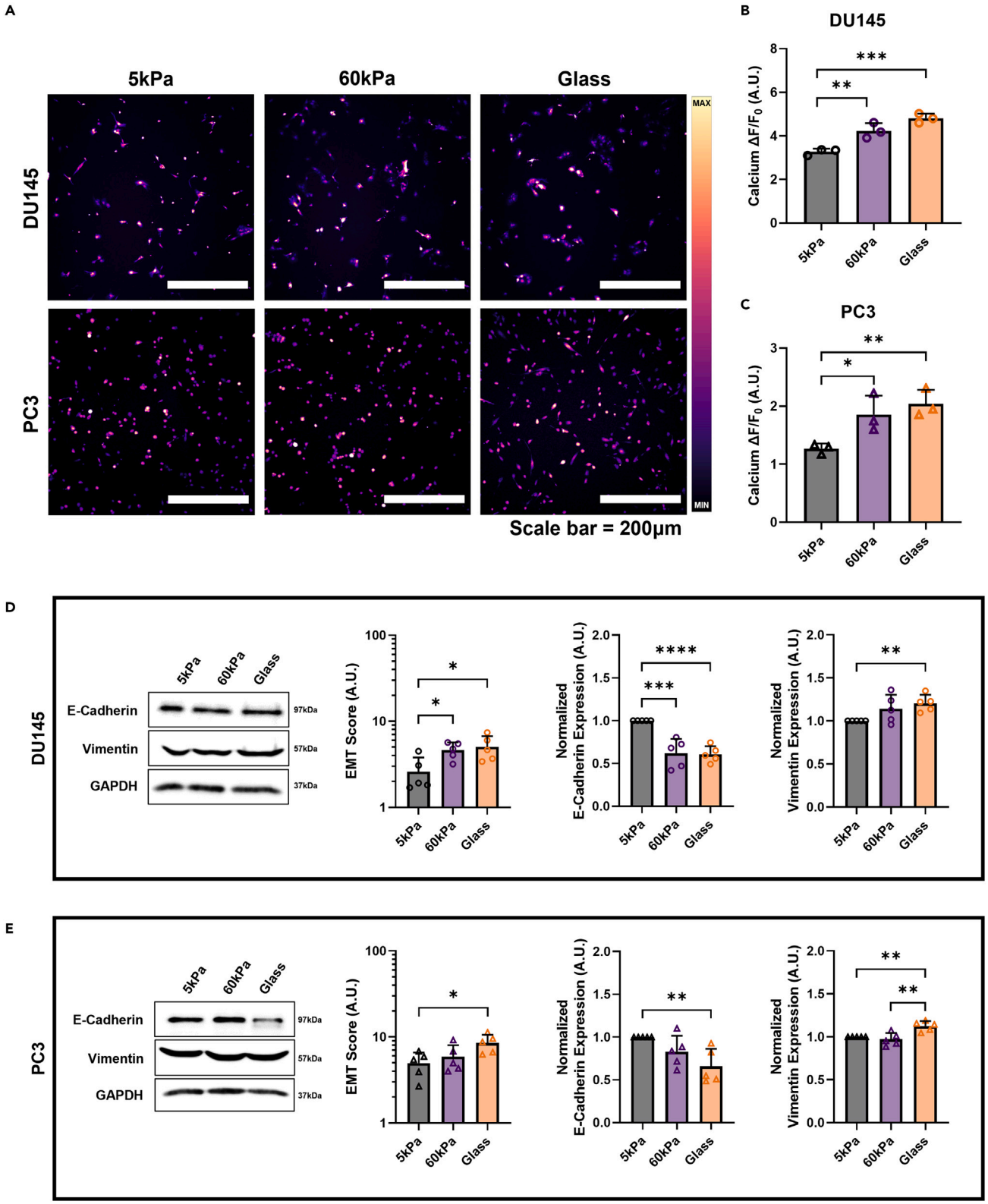
A
5kPa
60kPa
Glass
DU145
PC3
MAX
MIN
Scale bar = 200μm
B
DU145
Calcium ΔF/F0 (A.U.)
C
PC3
D
DU145
E-Cadherin
Vimentin
GAPDH
97kDa
57kDa
37kDa
EMT Score (A.U.)
Normalized E-Cadherin Expression (A.U.)
Normalized Vimentin Expression (A.U.)
E
PC3

Figure 1. Effect of stiffness on intracellular calcium concentration and EMT-related protein expression shifts

(A) Micrographs displaying the increase of Fluo-4 mean fluorescence with stiffness. Quantification of the changes in intracellular calcium concentration in cells grown on 5 kPa PA gels, 60 kPa PA gels, and the glass control in (B) DU145 cells and (C) PC3 cells. Western blot results for the (D) DU145 cells and (E) PC3 cells showing representative images and quantification of EMT Score (Vimentin/E-Cadherin), normalized vimentin expression, and normalized E-cadherin expression. Scale bar = 200 μm. Intracellular calcium concentration graphs display the mean ± SD for n=3. Western blot quantification graphs display the mean ± SD for n=5 replicates. Statistical significance is shown as * for $p < 0.05$, ** for $p < 0.01$, *** for $p < 0.001$, and **** for $p < 0.0001$, as evaluated by unpaired, parametric t-tests.

$\Delta F/F_0$ value for both of the cell lines on the two stiffer substrates were not statistically different from each other, suggesting that there is an upper limit to the mechanosensitivity of prostate cancer cells and subsequently a maximum threshold for intracellular calcium concentration because of changing stiffness.

Matrix stiffness had a pronounced effect on EMT-related protein expression. In both cell lines, an increase in stiffness led to significant increases in EMT score. This metric is calculated as the ratio of vimentin to E-cadherin expression. The DU145 cells showed significant increases in EMT ratio in the 60 kPa group and glass control substrate, compared to cells grown on the 5 kPa gels (Figure 1D). E-cadherin expression decreased by about 50% in both of these groups and vimentin expression was seen to increase significantly in the cells grown on the glass control. Protein expression in the PC3 cells was found to change similarly to the DU145 cells (Figure 1E). The greatest change in EMT score was found to occur between the cells grown on the 5 kPa PA gels and the glass control. E-cadherin expression was significantly decreased and vimentin expression significantly increased with increasing stiffness. This is consistent with other findings in the literature showing that vimentin expression is increased with stiffness.[27]

EMT-associated characteristics change with stiffness

The effect of matrix stiffness on cell shape and actin polymerization was investigated through fluorescence imaging of prostate cancer cells stained for DAPI and filamentous actin (F-actin). Micrographs depicting the DU145 cells can be seen in Figure 2A. Cell aspect ratio is a common metric for assessing changes in cell morphology: an increasing aspect ratio is associated with cells losing their apico-basal polarity and elongating to take on a more mesenchymal-like phenotype.[28,29] Manual contours of cells were measured to assess the aspect ratio. The mean aspect ratio of the DU145 cells increased significantly between the cells plated on the 60 kPa gels and the glass control substrate (Figure 2B). Of interest, F-actin fluorescence in the DU145 cells decreased significantly for the cells grown on both of the stiffer substrates compared to cells grown on the 5 kPa PA gels. In contrast, in the PC3 cells, the increases in matrix stiffness did influence the aspect ratio (Figure 2C). The difference was significant between the cells grown on the 5 kPa gels and the glass control, and show that, like the intracellular calcium concentration, it begins to plateau at higher stiffnesses. A decreasing trend in F-actin fluorescence was again observed with increasing stiffness, where cells grown on the softer gels showed significantly higher mean fluorescence than those grown on the stiffer gels.

Calcium steady-state concentration depends on treatment and stiffness

To investigate how changes in intracellular calcium concentration because of Piezo1 activation and inhibition affect important aspects of EMT, cells were treated with either Yoda1 or GsMTx-4 on each of the three substrates. Yoda1 is a specific pharmacological activator of Piezo1.[30] It decreases the mechanical threshold of activation of the channel by acting as a molecular wedge that allows for easier conformational changes because of deformation in the lipid bilayer. In contrast, GsMTx-4 can block Piezo1 and decrease calcium flux into the cell by stabilizing its closed state and therefore raising the energy barrier required to open the pore.[31] Yoda1 and GsMTx-4 treatment concentrations were chosen to match those used previously by our group.[24] Both treatments were utilized in all stiffness conditions to gain a more complete of how altering Piezo1 activity affects EMT progression.

Changes in intracellular calcium concentration due to treatments and matrix stiffness were confirmed with measurements of Fluo-4 fluorescence intensity using fluorescence microscopy. Piezo1 activation via the agonist Yoda1 had significant effects on DU145 cells grown on each of the three substrates in comparison to the DMSO vehicle control (Figure 3A). On the 5 kPa gels, 60 kPa gels, and the glass control the cells showed a 42%, 41%, and 36% increase, respectively, in $\Delta F/F_0$ with Yoda1 treatment compared to the DMSO control (Figure 3B). When the DU145 cells were treated with GsMTx-4, a significant decrease in intracellular calcium concentration was observed on both of the stiffer substrates compared to the DPBS control (Figure 3C). Pharmacological inactivation of Piezo1 did not have a significant effect on calcium $\Delta F/F_0$ in the DU145 cells grown on the 5 kPa gels.

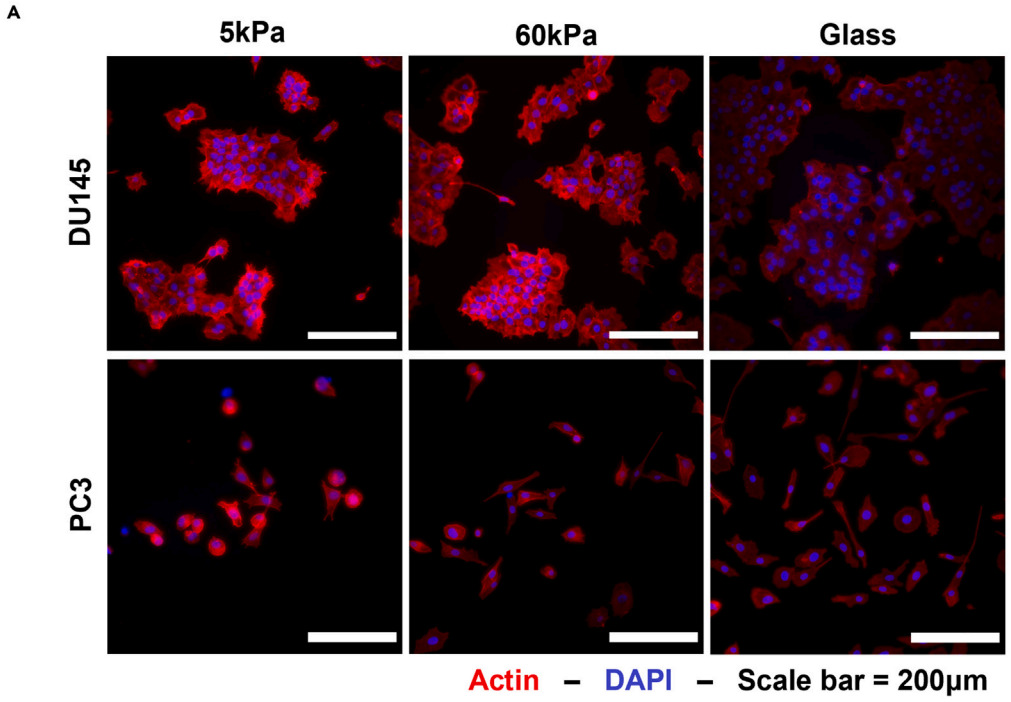
A
5kPa
60kPa
Glass
DU145
PC3
Actin – DAPI – Scale bar = 200μm

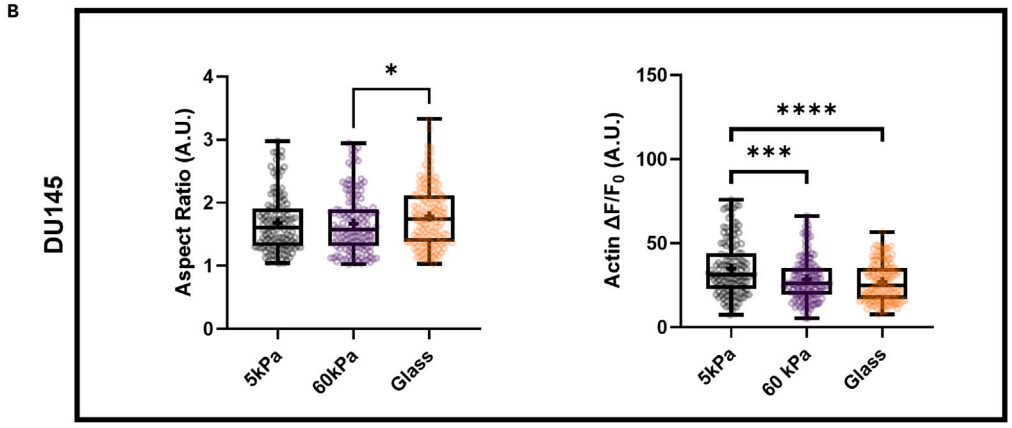
B
DU145
Aspect Ratio (A.U.)
Actin ΔF/F0 (A.U.)
5kPa
60kPa
60 kPa
Glass
*
***
****

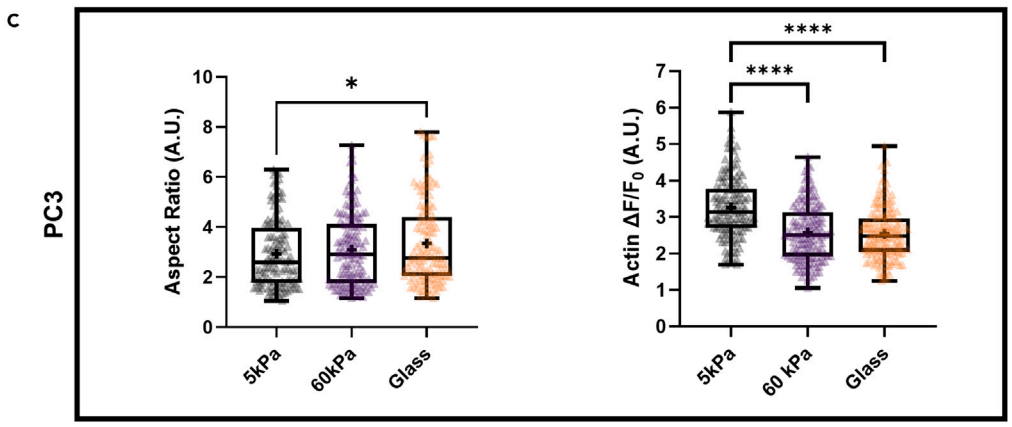
C
PC3
Aspect Ratio (A.U.)
Actin ΔF/F0 (A.U.)
5kPa
60kPa
60 kPa
Glass
*
****

Figure 2. Effect of stiffness on EMT morphology of prostate cancer cells

(A) Micrographs of DU145 and PC3 cells grown on the 3 different substrates and stained with ActinRed555 and DAPI. Quantification of increasing aspect ratio and decreasing F-actin fluorescence with stiffness in the (B) DU145 and (C) PC3 cells. Scale bar = 200 μm. Graphs display the boxplot from min to max of n = 50 sample size for each of the 3 biological replicates. Statistical significance is shown as * for $p < 0.05$, ** for $p < 0.01$, *** for $p < 0.001$, and **** for $p < 0.0001$, as evaluated by unpaired, parametric t-tests.

The results are summarized in Figure 3D, where the changes in cellular calcium steady-state concentration are compared between stiffnesses and treatment conditions. All the cells treated with Yoda1, on all of the substrate stiffnesses tested, had significantly increased intracellular calcium concentrations compared to the cells grown on the 5 kPa gels without treatment. Most noticeably, none of the untreated DU145 cells reached an equivalent intracellular calcium concentration as those cells treated with Yoda1. In addition, when the cells were treated with Yoda1 on the 5 kPa gels, they nearly reached the same magnitude of $\Delta F/F_0$ as those treated with Yoda1 on the stiffer substrates. The cells treated with GsMTx-4 on both of the stiffer substrates did not exhibit significantly different intracellular calcium concentrations to the untreated cells grown on the 5 kPa PA gels. This finding suggests that they also had a lower bound for Piezo1 inhibition.

Micrographs of the PC3 cell calcium steady-state results are presented in Figure 4A. The PC3 cells grown on the 5 kPa PA gel showed significantly increased intracellular calcium concentration when treated with Yoda1 compared to the DMSO vehicle control (Figure 4B). No difference was observed between the DMSO vehicle control and the Yoda1-treated cells on the glass control substrate or the 60 kPa PA gel. GsMTx-4 significantly decreased the calcium steady-state concentration on all three substrates (Figure 4C). The greatest difference was found in the cells incubated on the glass slides, where there was a 29% decrease in calcium steady-state concentration between the buffer vehicle control and the GsMTx-4 treatment. These results are summarized in Figure 4D, comparing the changes in cellular calcium steady-state concentration between stiffnesses and treatment conditions. The cells treated with Yoda1, on all substrate stiffnesses tested, had significantly increased intracellular calcium concentrations compared to the cells grown on the 5 kPa gels without treatment. In comparison, increasing matrix stiffness had no effect on intracellular calcium concentration when the cells were treated with GsMTx-4. These all showed a comparable magnitude of $\Delta F/F_0$ to untreated cells grown on the 5 kPa gels. Of interest, the intracellular calcium concentration did plateau around $\Delta F/F_0 \approx 2.4$ and exhibited a lower bound around $\Delta F/F_0 \approx 1.1$.

Effect of Yoda1 and GsMTx-4 on EMT-related protein expression

Western blotting was performed after the cells were treated with either Yoda1 or GsMTx-4 to determine how the changes in Piezo1 activation affect vimentin and E-cadherin expression. Qualitative western blot images of the effects of Piezo1 inhibition and activation on the prostate cancer cell line DU145 are shown in Figure 5A. When the DU145 cells were treated with Yoda1, there was a significant increase in EMT score across all the stiffness groups (Figure 5B). E-cadherin expression was reduced to almost undetectable levels at this condition, as evidenced by the significant decrease in fluorescent signal compared to the DMSO vehicle control. Vimentin expression was most affected in the cells grown on 5 kPa gels where there was a significant increase after Yoda1 treatment compared to the vehicle control. In comparison, GsMTx-4 only led to a decrease in EMT score in the glass control condition compared to the buffer control, although there were not any significant changes in individual protein expression (Figure 5C).

Results from the western blots of PC3 cells grown on the three substrates and treated with either Yoda1 or GsMTx-4 can be seen in Figure 6A. Similarly to the DU145 cells, the PC3 cells also showed a significant increase in EMT score when treated with Yoda1 compared to the DMSO control at all three matrix stiffness conditions (Figure 6B). E-cadherin expression was reduced by half in PC3 cells grown on each of the three substrates after Yoda1 treatment, compared to the control. Following the trends in calcium concentration, cells grown on 5 kPa gels showed a significant increase in vimentin expression when treated with Yoda1, compared to the DMSO vehicle control. Piezo1 inhibition via GsMTx-4, compared to the buffer control, significantly decreased the EMT score of PC3 cells grown on glass coverslips (Figure 6C). No significant changes in E-cadherin were observed with GsMTx-4 treatment, but vimentin expression was significantly reduced in the cells grown on glass control substrates compared to the vehicle control group.

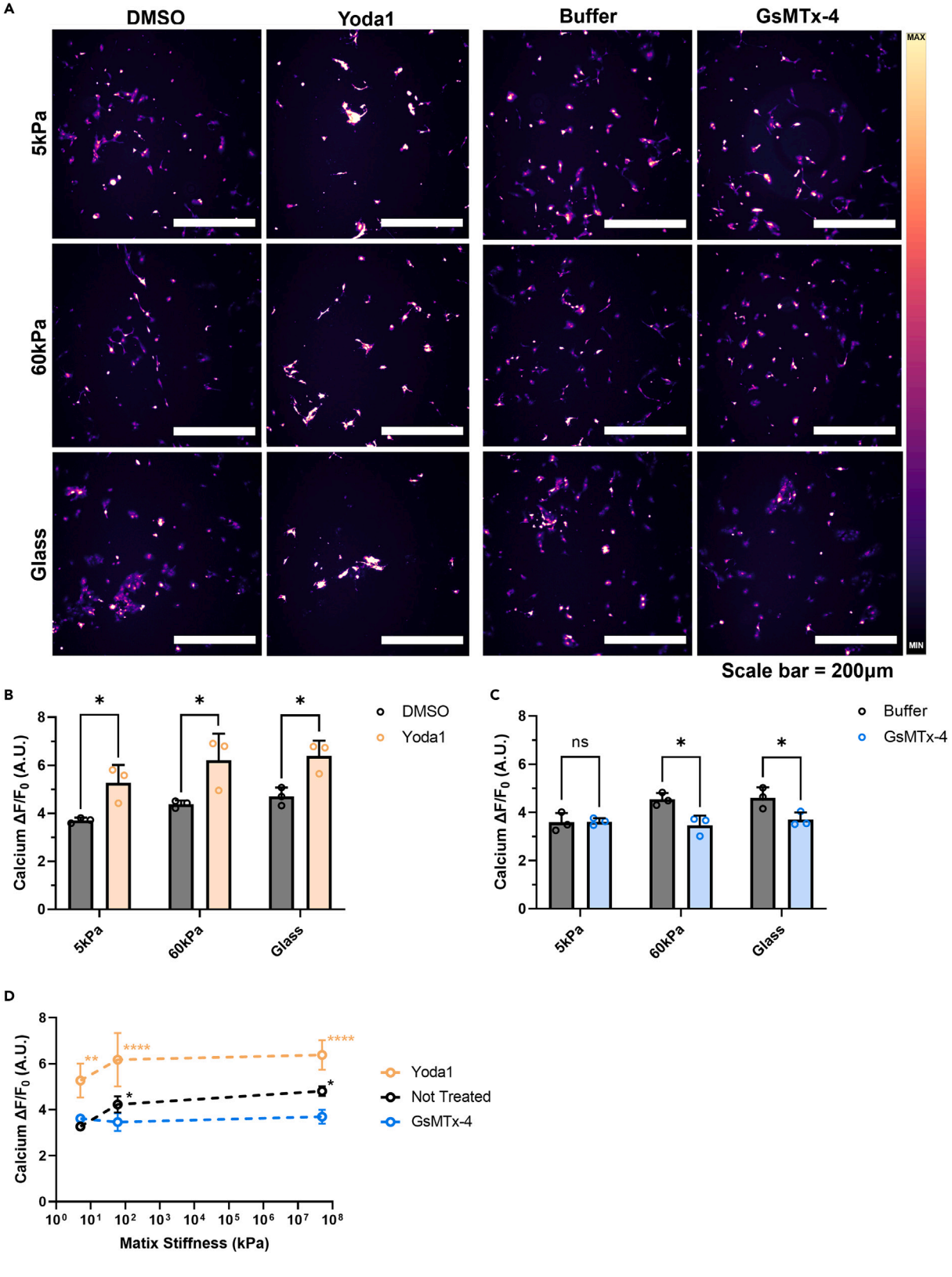
A
DMSO
Yoda1
Buffer
GsMTx-4
5kPa
60kPa
Glass
MAX
MIN
Scale bar = 200μm
B
Calcium ΔF/F0 (A.U.)
DMSO
Yoda1
5kPa
60kPa
Glass
C
Calcium ΔF/F0 (A.U.)
Buffer
GsMTx-4
ns
D
Calcium ΔF/F0 (A.U.)
Yoda1
Not Treated
GsMTx-4
Matix Stiffness (kPa)

Figure 3. Effects of pharmacological activation and inhibition on intracellular calcium concentration at different stiffnesses in DU145 cells

(A) Micrographs displaying Fluo-4 fluorescence of DU145 cells grown on 5 kPa, 60 kPa, and glass substrates and treated with Yoda1, GsMTx-4, and their vehicle controls (DMSO and buffer, respectively).

(B) Difference in intracellular calcium concentration between DMSO- and Yoda1-treated.

(C) Changes in $\Delta F/F_0$ with buffer or GsMTx-4 treatment of cells.

(D) Summary of pharmacological activation and inhibition of Piezo1 on soft and stiff gels, and the glass control compared to the cells that did not receive any treatment. Scale bar = 200 μm. Graphs display the mean ± SD for n = 3 replicates. Statistical significance is shown as * for $p < 0.05$, ** for $p < 0.01$, *** for $p < 0.001$, and **** for $p < 0.0001$, as evaluated by unpaired, parametric t-tests.

Effects of Yoda1 and GsMTx-4 on EMT morphology

DU145 and PC3 cells were stained with ActinRed555 to measure the changes in cell aspect ratio and F-actin fluorescence in response to the pharmacological activation of Piezo1 with Yoda1 at each of the different stiffnesses. The effects of pharmacological activation and inhibition of Piezo1 were prominent on DU145 cell morphology (Figure 7A). Yoda1 treatment led to a more elongated, mesenchymal-like cell shape and lower F-actin fluorescence in DU145 cells grown on the 5 kPa gels (Figure 7B). In the DU145 cells grown on the 5 kPa gels, the F-actin $\Delta F/F_0$ was 46% lower in the treatment group compared to the vehicle control. A significant increase in aspect ratio was seen in these cells when grown on the 60 kPa gels after Piezo1 activation via Yoda1. F-actin polymerization exhibited a significant decrease with Yoda1 treatment at this stiffness as well, although this was not as pronounced of a change as on the softer gels. No significant changes were observed between the treatment and control groups on the DU145 cells grown on the glass coverslips.

Consistent with the western blot results, the DU145 cells were found to be sensitive to the GsMTx-4 treatment when grown on the stiffer substrates (Figure 7C). On the 5 kPa substrates, there were no changes in the cell aspect ratio or F-actin $\Delta F/F_0$ between the GsMTx-4 treatment and control groups. As the stiffness increased to 60 kPa, the aspect ratio showed a significant decrease with Piezo1 inhibition compared to the buffer control. In addition, the $\Delta F/F_0$ increased significantly at this stiffness when Piezo1 was pharmacologically inhibited. These trends were also observed in the DU145 cells cultured on the glass control surface, although this difference was less pronounced.

Changes in EMT morphology in the PC3 cells when treated with Yoda1 were found to be more subtle (Figure 8A). Yoda1 had the greatest effect on the PC3 cells grown on the 5 kPa gels. At this stiffness condition, cells treated with the Piezo1 agonist were significantly more spindle-like and elongated than those in the vehicle control group (Figure 8B). A 22% decrease in F-actin fluorescence was observed at this stiffness when the cells were treated with Yoda1. In comparison, the cells grown on the 60 kPa gels and the glass control showed no significant changes in aspect ratio or mean F-actin fluorescence compared to the control. GsMTx-4 treatment did not have an effect on PC3 cells regardless of the substrate they were grown on (Figure 8C). No significant change in aspect ratio or F-actin fluorescence was observed between the buffer and GsMTx-4 treatment groups in cells grown on the 5 kPa gels, the 60 kPa gels, or the glass controls. These trends are consistent with the observations made in the changes in total vimentin expression of the PC3 cells with varying treatments and stiffness.

DISCUSSION

Changes in intracellular calcium concentrations are known to govern several important processes in cancer cells linked to disease progression, including increased proliferation, migration, invasion, resistance to apoptosis, and angiogenesis.[32–37] EMT and mechanotransduction are highly multidimensional and complex processes which rely on several different mechanisms to take place.[9,38] Cells have the ability to modulate calcium flux into the intracellular space via mechanosensitive ion channels in the membrane, such as Piezo1.[16] In the literature, Piezo1 has been associated with increased EMT in hepatocellular carcinoma by activating TGF-β signaling and in cholangiocarcinoma via the Hippo/YAP signaling axis.[39]

Piezo1 is opened by tension in the cell membrane as the matrix resists deformation when a cell pulls on it to migrate.[14] The present study connects how the increases in calcium concentration via Piezo1 channel opening because of increased matrix stiffness can lead to increased EMT in the prostate cancer cell lines DU145 and PC3. This environment was modeled by polymerizing PA gels of 5 kPa and 60 kPa which recapitulated the stiffnesses of healthy prostatic tissue and prostate cancer tumor, respectively (Figure S1).

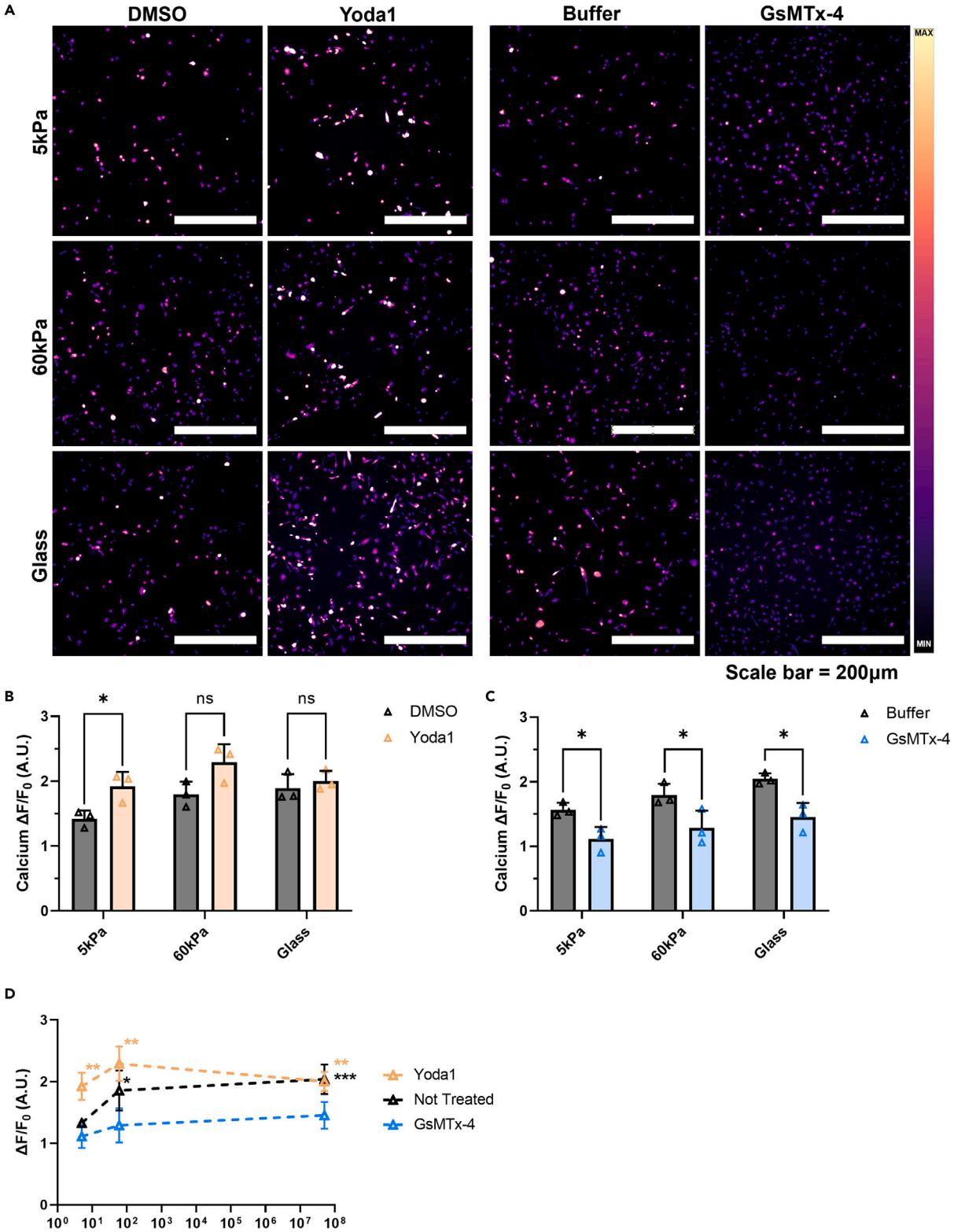
A
DMSO
Yoda1
Buffer
GsMTx-4
5kPa
60kPa
Glass
MAX
MIN
Scale bar = 200μm
B
Calcium ΔF/F0 (A.U.)
*
ns
ns
DMSO
Yoda1
5kPa
60kPa
Glass
C
Calcium ΔF/F0 (A.U.)
*
*
*
Buffer
GsMTx-4
5kPa
60kPa
Glass
D
ΔF/F0 (A.U.)
**
**
*
**
***
Yoda1
Not Treated
GsMTx-4
Matix Stiffness (kPa)

Figure 4. Effects of pharmacological activation and inhibition on intracellular calcium concentration at different stiffnesses in PC3 cells

(A) Micrographs displaying Fluo-4 fluorescence of PC3 cells grown on 5 kPa, 60 kPa, and glass substrates and treated with Yoda1, GsMTx-4, and the vehicle controls (DMSO and Buffer, respectively).

(B) Difference in intracellular calcium concentration between DMSO- and Yoda1-treated cells.

(C) Changes in $\Delta F/F_0$ with buffer or GsMTx-4 treatment of cells.

(D) Summary of pharmacological activation and inhibition of Piezo1 on soft and stiff gels, and the glass control compared to cells that did not receive any treatment. Scale bar = 200 μm. Graphs display the mean ± SD for n = 3 replicates. Statistical significance is shown as * for $p < 0.05$, ** for $p < 0.01$, *** for $p < 0.001$, and **** for $p < 0.0001$, as evaluated by unpaired, parametric t-tests.

Most cells in the human body are acutely sensitive to changes in intracellular calcium concentrations, as this governs most aspects of cellular life.[40] Cells utilize calcium channels as one of the main signaling mechanisms to sense changes in the extracellular space and convert these to reactions in the intracellular domain.[41] Once inside the cell, calcium regulates several signaling networks. It is heavily involved in

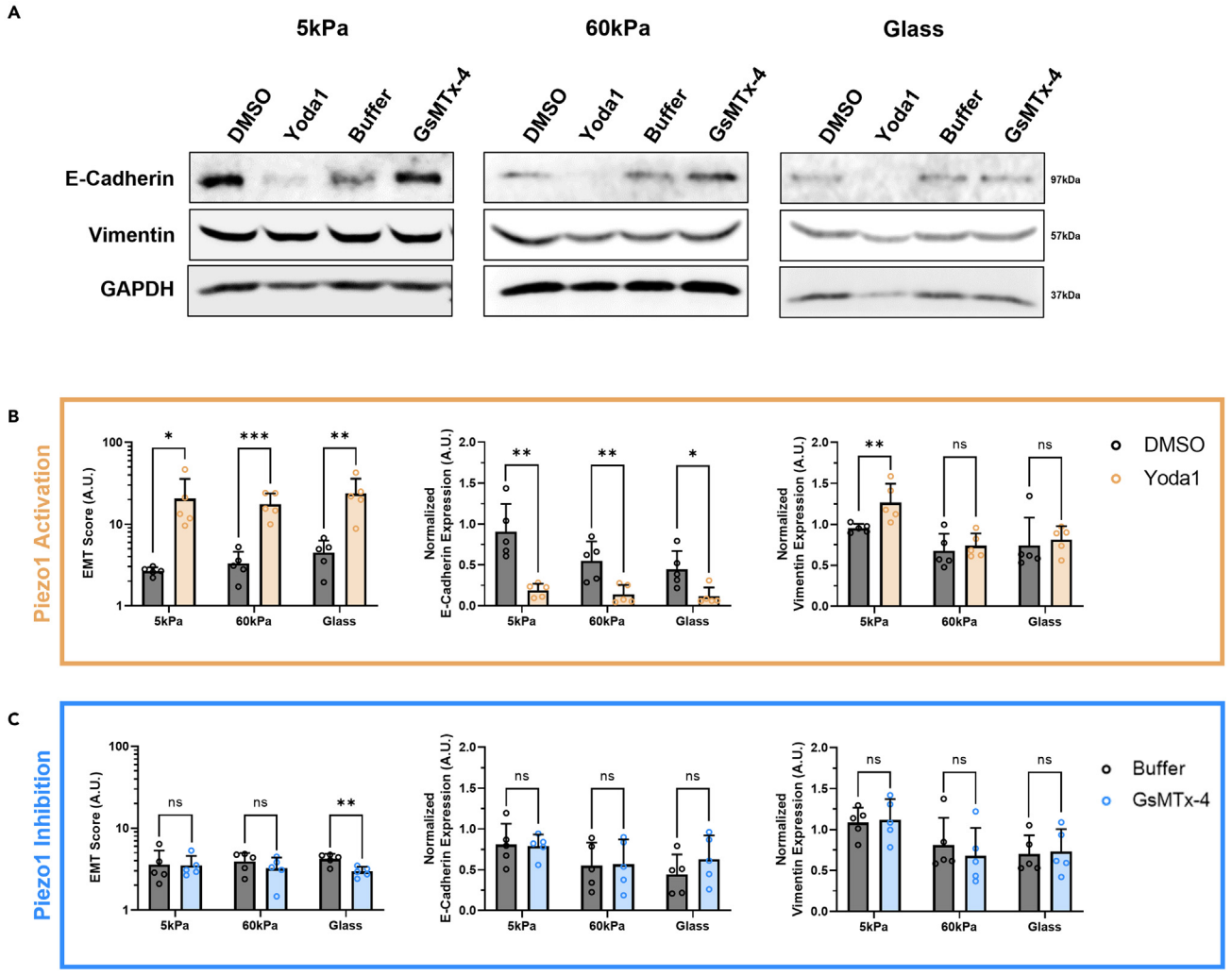

Figure 5. Western blots showing the effects of pharmacological activation and inhibition of Piezo1 on substrates of increasing stiffness on EMT-related protein expression in DU145 cells

(A) Qualitative images of the western blot results showing changing E-cadherin and vimentin expression in DU145 cells with matrix stiffness and treatments compared to the housekeeping protein GAPDH.

(B) Quantification of the western blot bands showing increasing EMT score, decreasing E-cadherin expression, and increasing vimentin expression in DU145 cells treated with Yoda1 compared to the DMSO vehicle control.

(C) Quantification of the western blot bands showing changes in EMT score, normalized E-cadherin expression, and normalized vimentin expression in DU145 cells treated with GsMTx-4 compared to the buffer vehicle control. Graphs display the mean ± SD for n=5 replicates normalized to the not treated, 5 kPa group. Statistical significance is shown as * for $p < 0.05$, ** for $p < 0.01$, *** for $p < 0.001$, and **** for $p < 0.0001$, as evaluated by unpaired, parametric t-tests.

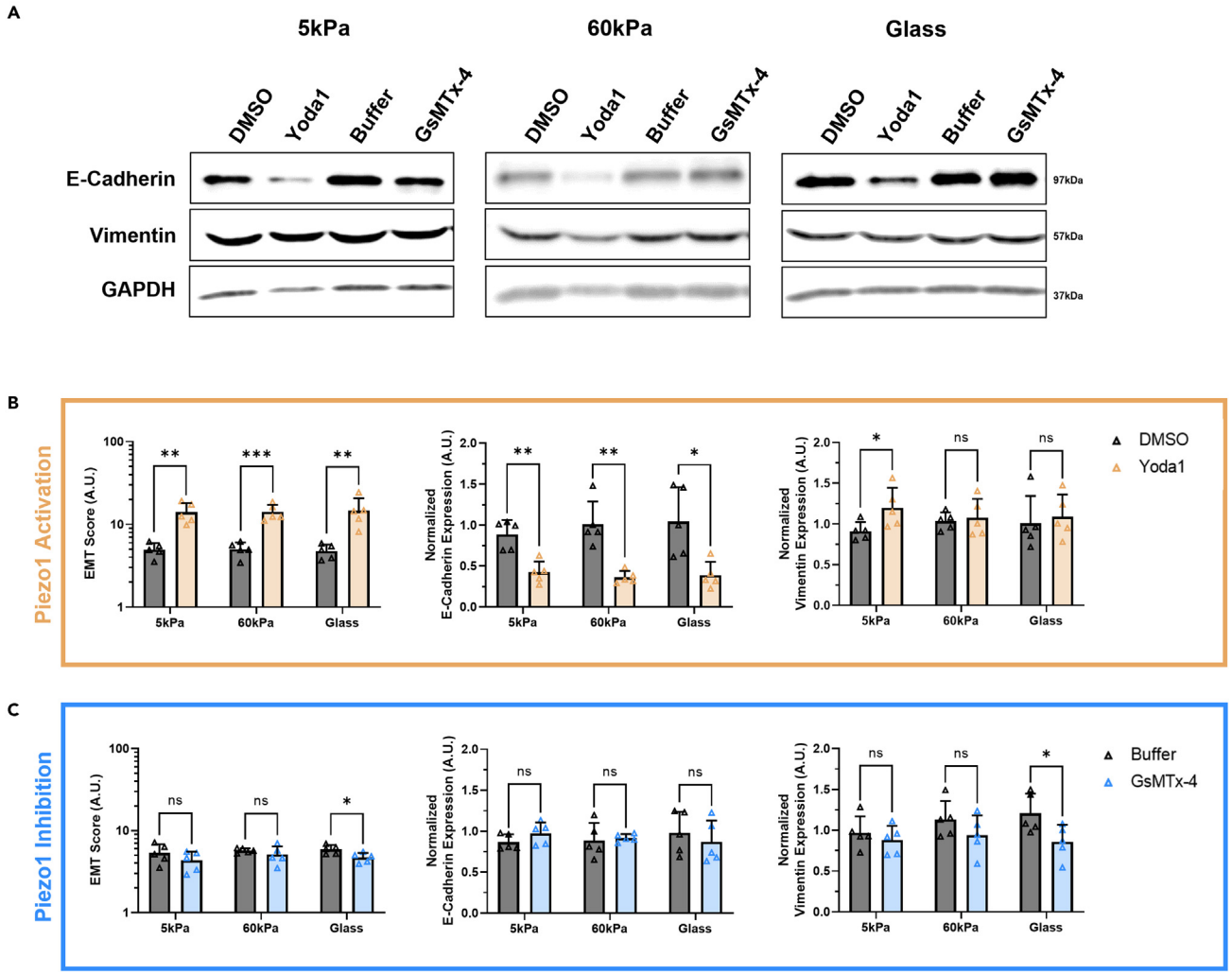

Figure 6. Western blots showing the effects of pharmacological activation and inhibition of Piezo1 on substrates of increasing stiffness on EMT-related protein expression in PC3 cells

(A) Qualitative images of the western blot results showing differential E-cadherin and vimentin expression in PC3 cells with matrix stiffness and treatments compared to GAPDH.

(B) Quantification of the western blot bands showing increasing EMT score, decreasing E-cadherin expression, and increasing vimentin expression in PC3 cells treated with Yoda1 compared to DMSO vehicle control.

(C) Quantification of the western blot bands showing changes in EMT score, normalized E-cadherin expression, and normalized vimentin expression in PC3 cells treated with GsMTx-4 compared to the buffer vehicle control. Graphs display the mean ± SD for n=5 replicates normalized to the not treated, 5 kPa group. Statistical significance is shown as * for $p < 0.05$, ** for $p < 0.01$, *** for $p < 0.001$, and **** for $p < 0.0001$, as evaluated by unpaired, parametric t-tests.

mitochondrial health and function, innate immunity, and cellular apoptosis pathways, which are sensitive to nano-to micro-molar scale changes in intracellular calcium concentration. As a result, the observed changes in calcium fluorescence in the DU145 and PC3 cell lines because of changing stiffness are significant, as seen in Figure 1. Of interest, the DU145 cells were found to be less sensitive to changes in matrix stiffness alone compared to the PC3 cells. Differences between the two cell lines chosen might also play a role in the slight variations of cell responses observed. This could be because of the fact that DU145 cells are known to have a higher cellular stiffness than PC3 cells, and thus may have the ability to resist deformation to a greater extent.[42] In terms of cell morphology, PC3 cells are naturally very spindle-like, and are seen in culture to grow more independently from each other. In comparison, DU145 cells tend to cluster in culture and have a more rounded cell shape. This difference suggests for more significant changes in EMT conversion to be observed in the DU145 cell line.

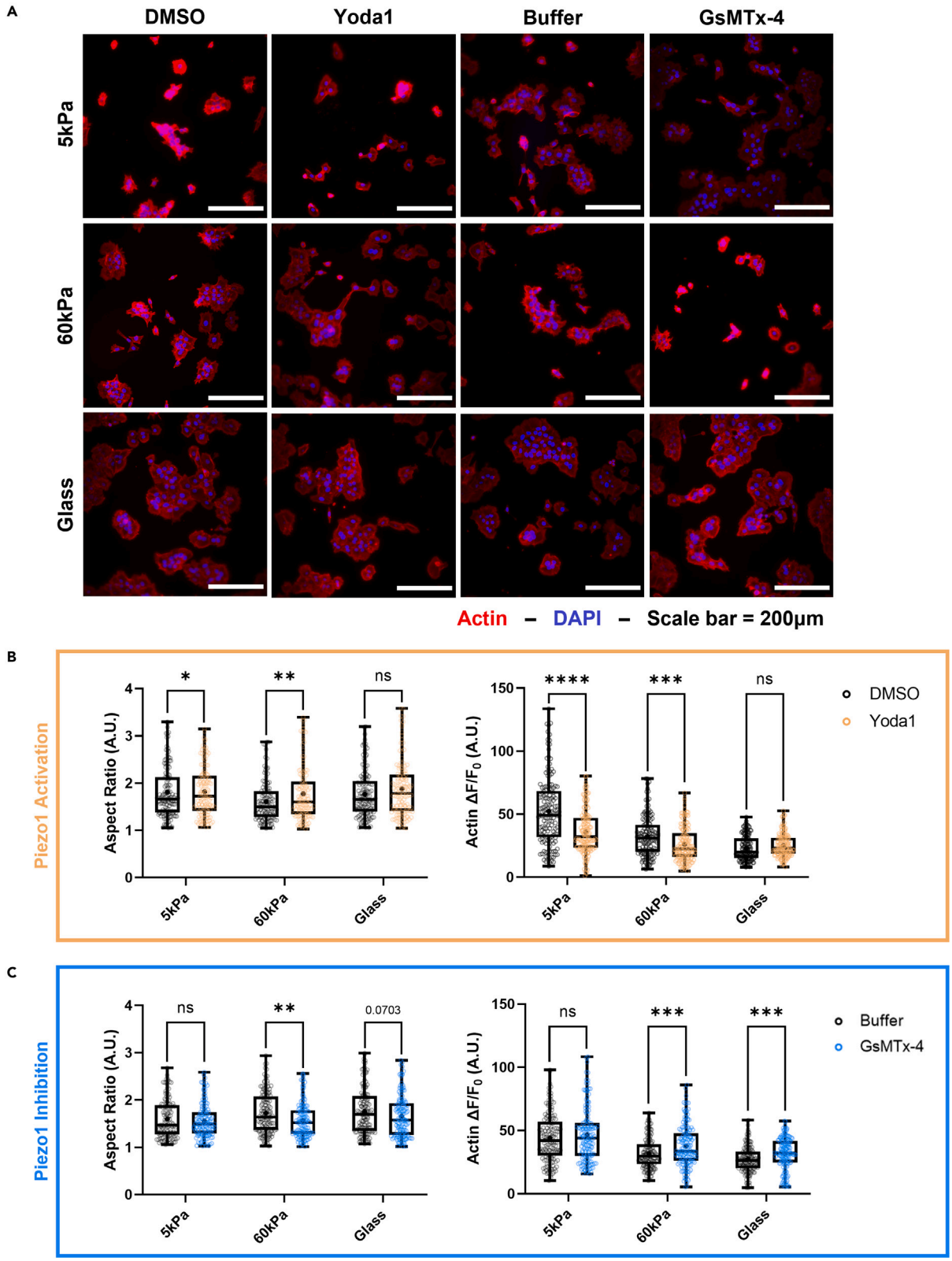
A
DMSO
Yoda1
Buffer
GsMTx-4
5kPa
60kPa
Glass
Actin – DAPI – Scale bar = 200μm
B
Piezo1 Activation
Aspect Ratio (A.U.)
Actin ΔF/F0 (A.U.)
*
**
ns
****
***
ns
5kPa
60kPa
Glass
DMSO
Yoda1
C
Piezo1 Inhibition
Aspect Ratio (A.U.)
Actin ΔF/F0 (A.U.)
ns
**
0.0703
ns
***
***
5kPa
60kPa
Glass
Buffer
GsMTx-4

Figure 7. Effects of Yoda1 treatment on the aspect ratio and F-actin fluorescence of DU145 cells incubated on substrates of increasing stiffness

(A) Micrographs showing DU145 cells on soft and hard PA gels, as well as the glass control stained with ActinRed555 and DAPI after treatments with Yoda1, GsMTx-4, and their vehicle controls (DMSO and buffer, respectively).

(B) Quantification of aspect ratio and F-actin fluorescence of the DU145 cells in each stiffness condition comparing Yoda1 treatment to the DMSO control.

(C) Quantification of aspect ratio and F-actin fluorescence in each stiffness condition comparing GsMTx-4 treatment to the buffer vehicle control. Scale bar = 200 μm. Graphs display the boxplot from min to max of n = 50 sample size for each of the 3 biological replicates. Statistical significance is shown as * for $p < 0.05$, ** for $p < 0.01$, *** for $p < 0.001$, and **** for $p < 0.0001$, as evaluated by unpaired, parametric t-tests.

In its resting state, Piezo1 takes on an inverted dome shape, storing potential energy in this way.[15] As cells migrate, they will pull against the matrix, which resists deformation proportionally to its stiffness. This response creates lateral membrane tension causing Piezo1 to transition into its open state by flattening proportionally. When the PC3 cells were plated on stiffer substrates, the measured calcium fluorescence plateaued, suggesting that the calcium channel had likely reached a maximum open state because of substrate resistance to deformation (Figure 1C). Yoda1 acts as a molecular wedge, decreasing the mechanical threshold for activation to increase the flow of calcium through the pore.[30] Therefore, when cells were treated with Yoda1 on the softer substrates, the calcium fluorescence increased significantly compared to the vehicle control (Figures 3 and 4). When PC3 cells were incubated on the stiffer substrates, treatment with Yoda1 did not increase calcium steady-state concentration because this had likely already reached a maximum open state. In contrast, DU145 cells did not appear to reach a maximum open state on glass coverslips because Yoda1 treatment caused a significant increase in calcium $\Delta F/F_0$ in this stiffness condition. Again, this supports the hypothesis that the higher cell stiffness was not able to fully activate Piezo1, thus allowing for a further increase in calcium steady-state concentration via the Yoda1 treatment. Conversely, GsMTx-4 gates Piezo1 to stabilize its closed state, in this way raising the energy barrier required to open the pore and decrease calcium steady-state concentration in the cell.[31] Therefore, GsMTx-4 was able to reduce the calcium steady-state concentration in the cells on all three substrate stiffnesses, especially on the stiffer gels where Piezo1 showed greater activity.

Vimentin expression and aspect ratio are two factors that have been heavily linked to EMT characterization in cancerous cells. In a study by *Leggett* et al., a modeling approach to EMT characterization based on vimentin expression and cytoplasm elongation was developed.[28] These morphological features were sufficient to accurately predict EMT phenotype in single cell analysis. In addition, EMT progression is known to be associated with a decrease in cell-cell junction proteins, such as E-cadherin.[43,44] Therefore, to understand the extent of EMT progression in DU145 and PC3 cells at each stiffness condition and after Piezo1 activation and inhibition, western blots were conducted to assess vimentin and E-cadherin expression. By treating DU145 and PC3 cells with Yoda1, increased vimentin expression (Figures 5 and 6), decreased E-cadherin expression, and increased aspect ratio (Figures 7 and 8) were observed compared to cells incubated with DMSO when grown on the softer substrates. Similar results were observed in the groups that received no treatment with only stiffness increased (Figures 1 and 2). Minimal changes in vimentin expression, E-cadherin expression, and aspect ratio were observed between the vehicle control and Yoda1 treatment in the cells cultured on glass because of the advanced state of EMT that high stiffness environments can induce on their own.

Two of the main cellular cytoskeletal elements are the actin stress fibers and vimentin intermediate filaments. These govern motility and structural integrity while working in concert, and heavily influence each other.[45] The study by *Jiu* et al. sheds light on how actin stress fiber assembly can be inhibited by vimentin filaments, and how knocking out vimentin via siRNAs will increase F-actin fluorescence. The results showing the decreasing F-actin fluorescence with increasing stiffness can be seen in Figure 2 in both cell lines. These trends match the increases in vimentin expression with Yoda1 treatment and the decreases in F-actin fluorescence compared to the vehicle control (Figures 7 and 8). Similarly, a study by Stournanaras et al. also reported observing that total actin and F-actin expression were decreased in malignant human lymphocytes compared to healthy lymphocytes.[46]

Pharmacologically inhibiting or knocking down the calcium channel TRPV4 are both known to prevent EMT morphology in breast cancer even at higher matrix stiffnesses.[39] Similar effects were observed in our study in DU145 prostate cancer cells after pharmacological inhibition of Piezo1 by quantifying EMT-related protein expression (Figure 5), aspect ratio, and F-actin fluorescence (Figure 7). Of interest, these trends were not observed when PC3 cells were treated with GsMTX-4 on the high stiffness substrates. In these groups, no significant changes in aspect ratio, F-actin fluorescence, or EMT-related protein expression were

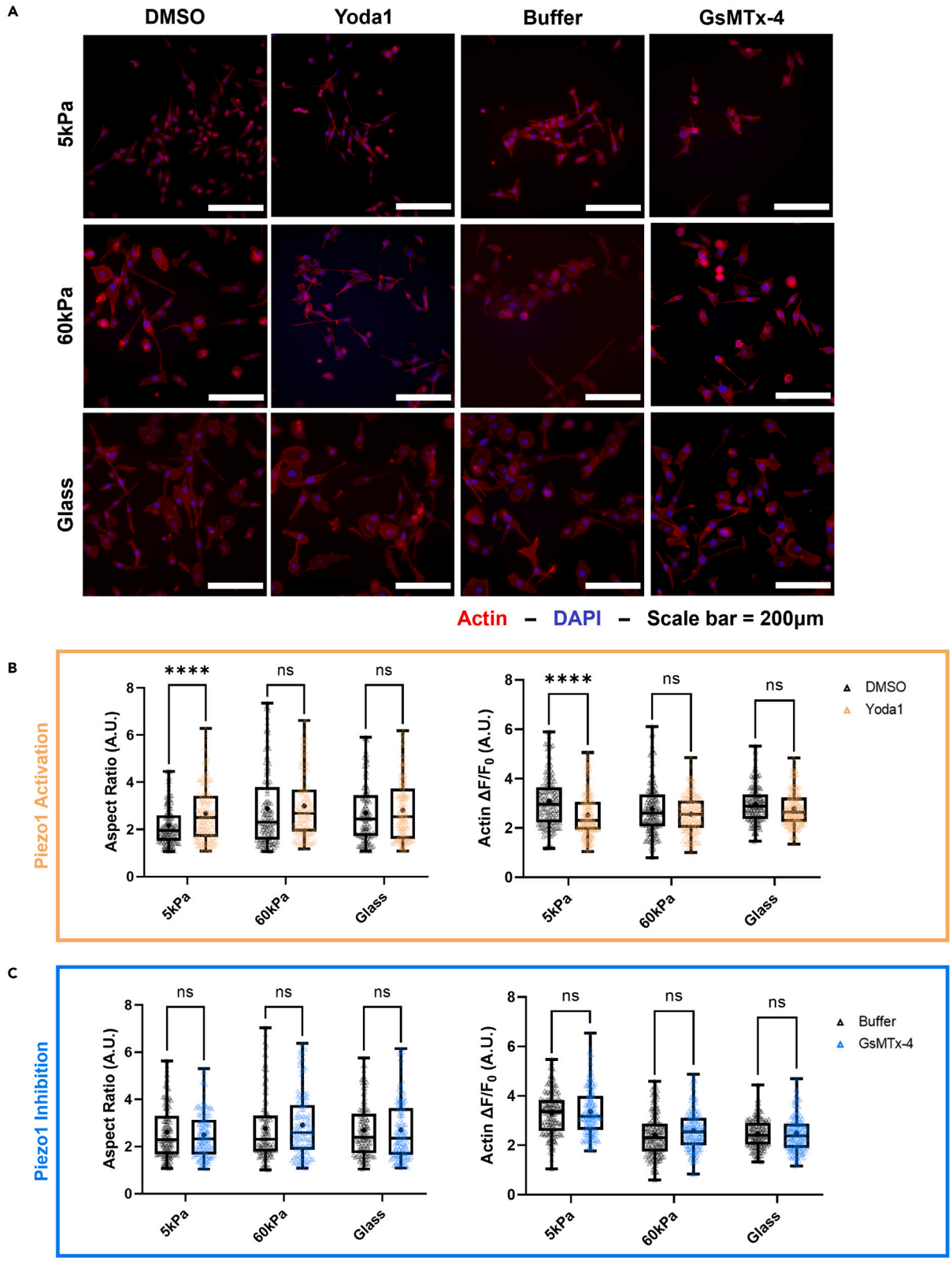
A
DMSO
Yoda1
Buffer
GsMTx-4
5kPa
60kPa
Glass
Actin – DAPI – Scale bar = 200μm
B
Piezo1 Activation
Aspect Ratio (A.U.)
Actin ΔF/F0 (A.U.)
****
ns
5kPa
60kPa
Glass
DMSO
Yoda1
C
Piezo1 Inhibition
Buffer
GsMTx-4

Figure 8. Effects of Yoda 1 treatment on the aspect ratio and F-actin fluorescence of PC3 cells incubated on substrates of increasing stiffness

(A) Micrographs showing PC3 cells on soft and hard PA gels, as well as the glass control stained with ActinRed555 and DAPI after treatments with Yoda1, GsMTx-4, and their vehicle controls (DMSO and Buffer, respectively).

(B) Quantification of aspect ratio and F-actin fluorescence of the PC3 cells in each stiffness condition comparing Yoda1 treatment to the DMSO control.

(C) Quantification of aspect ratio and F-actin fluorescence at each stiffness condition comparing GsMTx-4 treatment to the buffer vehicle control. Scale bar = 200 μm. Graphs display the boxplot from min to max of n = 50 sample size for each of the 3 biological replicates. Statistical significance is shown as * for $p < 0.05$, ** for $p < 0.01$, *** for $p < 0.001$, and **** for $p < 0.0001$, as evaluated by unpaired, parametric t-tests.

observed. This finding could be because of alternative integrin signaling pathways becoming activated at the higher substrate stiffness and circumventing the pharmacological inhibition of Piezo1.[47] EMT and mechanotransduction are highly multidimensional and complex processes which rely on several different mechanisms to take place.[9,38] Piezo1 activation had profound effects in promoting EMT characteristics, yet its pharmacological inhibition did not have an effect. Therefore, this suggests that it is an important component in cell sensing of the matrix stiffness and the subsequent activation of EMT pathways but is not solely responsible for this sensing.

Of interest, when cells are exposed to fluid stress in the circulation, the forces they experience lead to increases in intracellular calcium concentration in many different cell types, including cancerous cells.[48–51] The study by *Choi* et al. demonstrated that the high shear forces in the circulation were linked to increased EMT in circulating tumor cells isolated from breast cancer patients.[52] Shear stress was found to be a critical factor in the EMT conversion, leading to increased mesenchymal markers and increased tumor growth in an orthotopic mouse model of breast cancer. A parallel may be drawn from that work to this study, because it supports the hypothesis that forces from the extracellular environment cause changes in intracellular calcium concentrations thus leading to EMT.

In this study, the biophysical environment of a prostate cancer tumor was modeled using PA gels which recapitulated the different stiffnesses observed during disease progression. The prostate cancer cell lines DU145 and PC3 were used to study the effects that the changes in stiffness had on EMT via Piezo1 modulation of calcium flux. It was seen in both cell lines that pharmacologically activating Piezo1 via Yoda1 treatment led to greater intracellular calcium concentrations, higher vimentin expression, increased aspect ratio, and lower F-actin fluorescence, especially at the softer PA gel condition. The opposite effect was seen in the stiffer substrates when cells were treated with the Piezo1 antagonist GsMTx-4. Overall, this study concludes that Piezo1 regulated calcium flux plays a key role in prostate cancer cell metastatic potential by sensing changes in ECM stiffness and modulating EMT markers.

Limitations of the study

In this study, PA gels coated in collagen were utilized to model the biophysical environment of a prostate cancer tumor. A current limitation to our study is the lack of genetic manipulation of Piezo1. A Piezo1 KD or KO would help elucidate whether Piezo1 is necessary for EMT characteristics to arise as prostate tissue stiffness increases during disease progression. Yet there are many other stretch-activated calcium channels, such as TRPV-4, which are also able to sense changes in matrix stiffness and have been shown to induce EMT.[39] The peptide GsMTx-4 was utilized because it is a selective inhibitor of cationic mechanosensitive ion channels, including both the TRP and Piezo channels.[53] In this way, we were able to determine what changes in cell morphology and protein expression because of stiffness occurred in the absence of cationic mechanosensitive ion channel activation. An emphasis is placed on the effects that Piezo1 specifically has on EMT progression by treating with Yoda1, which is highly potent and has a high binding specificity for Piezo1.[30]

STAR★METHODS

Detailed methods are provided in the online version of this paper and include the following:

- KEY RESOURCES TABLE
- RESOURCE AVAILABILITY
  - Lead contact
  - Materials availability
  - Data and code availability
- EXPERIMENTAL MODEL AND SUBJECT DETAILS
  - Cell culture and reagents
  - Polyacrylamide gel preparation

- METHOD DETAILS
  - Calcium imaging
  - Cell shape and actin polymerization assay
  - Western blotting
- QUANTIFICATION AND STATISTICAL ANALYSIS

SUPPLEMENTAL INFORMATION

Supplemental information can be found online at https://doi.org/10.1016/j.isci.2023.106275.

ACKNOWLEDGMENTS

PA gel crosslinker application for PA gel collagen coating was conducted at the Vanderbilt Institute of Nanoscale Science and Engineering. We are grateful for the support in PA gel polymerization and coating from Tin Nguyen and Ava Cassidy. This work was supported by the National Institutes of Health National Cancer Institute grant number CA203991.

AUTHOR CONTRIBUTIONS

Conceptualization: M.R.K., M.L.C., and J.M.H.; Formal analysis: M.L.C., S.B.H., N.T.R., and J.D.G.; Investigation: M.L.C., S.B.H., J.M.H., N.T.R., S.C.S., and J.A.V.; Methods provided: C.A.R.K.; Writing (original draft): M.L.C.; Writing (review and editing): M.R.K. and M.L.C.; Funding acquisition: M.R.K.; Supervision: M.R.K

DECLARATION OF INTERESTS

The authors declare no competing interests.

INCLUSION AND DIVERSITY

We support inclusive, diverse, and equitable conduct of research. One or more of the authors of this paper self-identifies as an underrepresented ethnic minority in their field of research or within their geographical location. One or more of the authors of this paper self-identifies as a gender minority in their field of research. One or more of the authors of this paper received support from a program designed to increase minority representation in their field of research.

Received: June 7, 2022
Revised: January 21, 2023
Accepted: February 18, 2023
Published: February 25, 2023

REFERENCES

1. Jolly, M.K., Ware, K.E., Gilja, S., Somarelli, J.A., and Levine, H. (2017). EMT and MET: necessary or permissive for metastasis? Mol. Oncol. *11*, 755–769. https://doi.org/10.1002/1878-0261.12083.

2. Kalluri, R., and Weinberg, R.A. (2009). The basics of epithelial-mesenchymal transition. J. Clin. Invest. *119*, 1420–1428. https://doi.org/10.1172/JCI39104.

3. Heerboth, S., Housman, G., Leary, M., Longacre, M., Byler, S., Lapinska, K., Willbanks, A., and Sarkar, S. (2015). EMT and tumor metastasis. Clin. Transl. Med. *4*, 6. https://doi.org/10.1186/s40169-015-0048-3.

4. Roche, J. (2018). The epithelial-to-mesenchymal transition in cancer. Cancers *10*, 52. https://doi.org/10.3390/cancers10020052.

5. Emon, B., Bauer, J., Jain, Y., Jung, B., and Saif, T. (2018). Biophysics of tumor microenvironment and cancer metastasis - a mini review. Comput. Struct. Biotechnol. J. *16*, 279–287. https://doi.org/10.1016/j.csbj.2018.07.003.

6. Bauer, J., Emon, M.A.B., Staudacher, J.J., Thomas, A.L., Zessner-Spitzenberg, J., Mancinelli, G., Krett, N., Saif, M.T., and Jung, B. (2020). Increased stiffness of the tumor microenvironment in colon cancer stimulates cancer associated fibroblast-mediated prometastatic activin A signaling. Sci. Rep. *10*, 50. https://doi.org/10.1038/s41598-019-55687-6.

7. Chen, W., Park, S., Patel, C., Bai, Y., Henary, K., Raha, A., Mohammadi, S., You, L., and Geng, F. (2021). The migration of metastatic breast cancer cells is regulated by matrix stiffness via YAP signalling. Heliyon *7*, e06252. https://doi.org/10.1016/j.heliyon.2021.e06252.

8. Schrader, J., Gordon-Walker, T.T., Aucott, R.L., van Deemter, M., Quaas, A., Walsh, S., Benten, D., Forbes, S.J., Wells, R.G., and Iredale, J.P. (2011). Matrix stiffness modulates proliferation, chemotherapeutic response, and dormancy in hepatocellular carcinoma cells. Hepatology *53*, 1192–1205. https://doi.org/10.1002/hep.24108.

9. Wullkopf, L., West, A.-K.V., Leijnse, N., Cox, T.R., Madsen, C.D., Oddershede, L.B., and Erler, J.T. (2018). Cancer cells' ability to mechanically adjust to extracellular matrix stiffness correlates with their invasive potential. Mol. Biol. Cell *29*, 2378–2385. https://doi.org/10.1091/mbc.E18-05-0319.

10. Barr, R.G., Memo, R., and Schaub, C.R. (2012). Shear wave ultrasound elastography of the prostate: initial results. Ultrasound Q. *28*, 13–20. https://doi.org/10.1097/RUQ.0b013e318249f594.

11. Ji, Y., Ruan, L., Ren, W., Dun, G., Liu, J., Zhang, Y., and Wan, Q. (2019). Stiffness of prostate gland measured by transrectal real-time shear wave elastography for detection of prostate cancer: a feasibility study. Br. J. Radiol. *92*, 20180970. https://doi.org/10.1259/bjr.20180970.

12. Rouvière, O., Melodelima, C., Hoang Dinh, A., Bratan, F., Pagnoux, G., Sanzalone, T., Crouzet, S., Colombel, M., Mège-Lechevallier, F., and Souchon, R. (2017). Stiffness of benign and malignant prostate tissue measured by shear-wave elastography: a preliminary study. Eur. Radiol. *27*, 1858–1866. https://doi.org/10.1007/s00330-016-4534-9.

13. Correas, J.-M., Tissier, A.-M., Khairoune, A., Vassiliu, V., Méjean, A., Hélénon, O., Memo, R., and Barr, R.G. (2015). Prostate cancer: diagnostic performance of real-time shear-wave elastography. Radiology *275*, 280–289. https://doi.org/10.1148/radiol.14140567.

14. Janmey, P.A., Fletcher, D.A., and Reinhart-King, C.A. (2019). Stiffness sensing by cells. Physiol. Rev. *100*, 695–724. https://doi.org/10.1152/physrev.00013.2019.

15. Coste, B., Xiao, B., Santos, J.S., Syeda, R., Grandl, J., Spencer, K.S., Kim, S.E., Schmidt, M., Mathur, J., Dubin, A.E., et al. (2012). Piezo proteins are pore-forming subunits of mechanically activated channels. Nature *483*, 176–181. https://doi.org/10.1038/nature10812.

16. Coste, B., Mathur, J., Schmidt, M., Earley, T.J., Ranade, S., Petrus, M.J., Dubin, A.E., and Patapoutian, A. (2010). Piezo1 and Piezo2 are essential components of distinct mechanically-activated cation channels. Science *330*, 55–60.

17. Dombroski, J.A., Hope, J.M., Sarna, N.S., and King, M.R. (2021). Channeling the force: Piezo1 mechanotransduction in cancer metastasis. Cells *10*, 2815. https://doi.org/10.3390/cells10112815.

18. Lin, Y.-C., Guo, Y.R., Miyagi, A., Levring, J., MacKinnon, R., and Scheuring, S. (2019). Force-induced conformational changes in Piezo1. Nature *573*, 230–234. https://doi.org/10.1038/s41586-019-1499-2.

19. Ellefsen, K.L., Holt, J.R., Chang, A.C., Nourse, J.L., Arulmoli, J., Mekhdjian, A.H., Abuwarda, H., Tombola, F., Flanagan, L.A., Dunn, A.R., et al. (2019). Myosin-II mediated traction forces evoke localized Piezo1-dependent Ca2+ flickers. Commun. Biol. *2*, 298. https://doi.org/10.1038/s42003-019-0514-3.

20. Wang, J., Jiang, J., Yang, X., Zhou, G., Wang, L., and Xiao, B. (2022). Tethering Piezo channels to the actin cytoskeleton for mechanogating via the cadherin-β-catenin mechanotransduction complex. Cell Rep. *38*, 110342. https://doi.org/10.1016/j.celrep.2022.110342.

21. Fang, X.-Z., Zhou, T., Xu, J.-Q., Wang, Y.-X., Sun, M.-M., He, Y.-J., Pan, S.-W., Xiong, W., Peng, Z.-K., Gao, X.-H., and Shang, Y. (2021). Structure, kinetic properties and biological function of mechanosensitive Piezo channels. Cell Biosci. *11*, 13. https://doi.org/10.1186/s13578-020-00522-z.

22. Han, Y., Liu, C., Zhang, D., Men, H., Huo, L., Geng, Q., Wang, S., Gao, Y., Zhang, W., Zhang, Y., and Jia, Z. (2019). Mechanosensitive ion channel Piezo1 promotes prostate cancer development through the activation of the Akt/mTOR pathway and acceleration of cell cycle. Int. J. Oncol. *55*, 629–644. https://doi.org/10.3892/ijo.2019.4839.

23. Chen, X., Wanggou, S., Bodalia, A., Zhu, M., Dong, W., Fan, J.J., Yin, W.C., Min, H.-K., Hu, M., Draghici, D., et al. (2018). A feedforward mechanism mediated by mechanosensitive ion channel Piezo1 and tissue mechanics promotes glioma aggression. Neuron *100*, 799–815.e7. https://doi.org/10.1016/j.neuron.2018.09.046.

24. Hope, J.M., Lopez-Cavestany, M., Wang, W., Reinhart-King, C.A., and King, M.R. (2019). Activation of Piezo1 sensitizes cells to TRAIL-mediated apoptosis through mitochondrial outer membrane permeability. Cell Death Dis. *10*, 837. https://doi.org/10.1038/s41419-019-2063-6.

25. Mitchell, M.J., and King, M.R. (2013). Fluid shear stress sensitizes cancer cells to receptor-mediated apoptosis via trimeric death receptors. New J. Phys. *15*, 015008. https://doi.org/10.1088/1367-2630/15/1/015008.

26. Lima, A.R., Araújo, A.M., Pinto, J., Jerónimo, C., Henrique, R., Bastos, M.d.L., Carvalho, M., and Guedes de Pinho, P. (2018). Discrimination between the human prostate normal and cancer cell exometabolome by GC-MS. Sci. Rep. *8*, 5539. https://doi.org/10.1038/s41598-018-23847-9.

27. Rice, A.J., Cortes, E., Lachowski, D., Cheung, B.C.H., Karim, S.A., Morton, J.P., and Del Río Hernández, A. (2017). Matrix stiffness induces epithelial–mesenchymal transition and promotes chemoresistance in pancreatic cancer cells. Oncogenesis *6*, e352. https://doi.org/10.1038/oncsis.2017.54.

28. Leggett, S.E., Sim, J.Y., Rubins, J.E., Neronha, Z.J., Williams, E.K., and Wong, I.Y. (2016). Morphological single cell profiling of the epithelial–mesenchymal transition. Integr. Biol. *8*, 1133–1144. https://doi.org/10.1039/C6IB00139D.

29. Ondeck, M.G., Kumar, A., Placone, J.K., Plunkett, C.M., Matte, B.F., Wong, K.C., Fattet, L., Yang, J., and Engler, A.J. (2019). Dynamically stiffened matrix promotes malignant transformation of mammary epithelial cells via collective mechanical signaling. Proc. Natl. Acad. Sci. USA *116*, 3502–3507. https://doi.org/10.1073/pnas.1814204116.

30. Botello-Smith, W.M., Jiang, W., Zhang, H., Ozkan, A.D., Lin, Y.-C., Pham, C.N., Lacroix, J.J., and Luo, Y. (2019). A mechanism for the activation of the mechanosensitive Piezo1 channel by the small molecule Yoda1. Nat. Commun. *10*, 4503. https://doi.org/10.1038/s41467-019-12501-1.

31. Bae, C., Sachs, F., and Gottlieb, P.A. (2011). The mechanosensitive ion channel Piezo1 is inhibited by the peptide GsMTx4. Biochemistry *50*, 6295–6300. https://doi.org/10.1021/bi200770q.

32. Holt, J.R., Zeng, W.-Z., Evans, E.L., Woo, S.-H., Ma, S., Abuwarda, H., Loud, M., Patapoutian, A., and Pathak, M.M. (2020). PIEZO1-induced cellular retraction controls keratinocyte migration in wound healing. Preprint at bioRxiv. https://doi.org/10.1101/2020.10.18.344598.

33. Kaur, J., and Sanyal, S.N. (2011). Intracellular pH and calcium signaling as molecular targets of diclofenac-induced apoptosis against colon cancer. Eur. J. Cancer Prev. *20*, 263–276. https://doi.org/10.1097/CEJ.0b013e3283431c25.

34. Fiorio Pla, A., Genova, T., Pupo, E., Tomatis, C., Genazzani, A., Zaninetti, R., and Munaron, L. (2010). Multiple roles of protein kinase A in arachidonic acid–mediated Ca2+ entry and tumor-derived human endothelial cell migration. Mol. Cancer Res. *8*, 1466–1476. https://doi.org/10.1158/1541-7786.MCR-10-0002.

35. Fiorio Pla, A., Ong, H.L., Cheng, K.T., Brossa, A., Bussolati, B., Lockwich, T., Paria, B., Munaron, L., and Ambudkar, I.S. (2012). TRPV4 mediates tumor-derived endothelial cell migration via arachidonic acid-activated actin remodeling. Oncogene *31*, 200–212. https://doi.org/10.1038/onc.2011.231.

36. Stewart, T.A., Yapa, K.T., and Monteith, G.R. (2015). Altered calcium signaling in cancer cells. Biochim. Biophys. Acta *1848*, 2502–2511. https://doi.org/10.1016/j.bbamem.2014.08.016.

37. Zhu, H., Zhang, H., Jin, F., Fang, M., Huang, M., Yang, C.S., Chen, T., Fu, L., and Pan, Z. (2014). Elevated Orai1 expression mediates tumor-promoting intracellular Ca2+ oscillations in human esophageal squamous cell carcinoma. Oncotarget *5*, 3455–3471. https://doi.org/10.18632/oncotarget.1903.

38. Kalli, M., and Stylianopoulos, T. (2018). Defining the role of solid stress and matrix stiffness in cancer cell proliferation and metastasis. Front. Oncol. *8*, 55. https://doi.org/10.3389/fonc.2018.00055.

39. Sharma, S., Goswami, R., and Rahaman, S.O. (2019). The TRPV4-TAZ mechanotransduction signaling Axis in matrix stiffness- and tgfβ1-induced epithelial-mesenchymal transition. Cell. Mol. Bioeng. *12*, 139–152. https://doi.org/10.1007/s12195-018-00565-w.

40. Clapham, D.E. (2007). Calcium signaling. Cell *131*, 1047–1058. https://doi.org/10.1016/j.cell.2007.11.028.

41. Hope, J.M., Greenlee, J.D., and King, M.R. (2018). Mechanosensitive ion channels: TRPV4 and P2X7 in disseminating cancer cells. Cancer J. *24*, 84–92. https://doi.org/10.1097/PPO.0000000000000312.

42. Hope, J.M., Bersi, M.R., Dombroski, J.A., Clinch, A.B., Pereles, R.S., Merryman, W.D., and King, M.R. (2021). Circulating prostate cancer cells have differential resistance to fluid shear stress-induced cell death. J. Cell Sci. *134*, jcs251470. https://doi.org/10.1242/jcs.251470.

43. Chunthapong, J., Seftor, E.A., Khalkhali-Ellis, Z., Seftor, R.E.B., Amir, S., Lubaroff, D.M., Heidger, P.M., and Hendrix, M.J.C. (2004). Dual roles of E-cadherin in prostate cancer invasion. J. Cell. Biochem. *91*, 649–661. https://doi.org/10.1002/jcb.20032.

44. Wang, W., Wang, L., Mizokami, A., Shi, J., Zou, C., Dai, J., Keller, E.T., Lu, Y., and Zhang, J. (2017). Down-regulation of E-cadherin enhances prostate cancer chemoresistance via Notch signaling. Chin. J. Cancer *36*, 35. https://doi.org/10.1186/s40880-017-0203-x.

45. Jiu, Y., Peränen, J., Schaible, N., Cheng, F., Eriksson, J.E., Krishnan, R., and Lappalainen, P. (2017). Vimentin intermediate filaments control actin stress fiber assembly through GEF-H1 and RhoA. J. Cell Sci. *130*, 892–902. https://doi.org/10.1242/jcs.196881.

46. Stournaras, C., Stiakaki, E., Koukouritaki, S.B., Theodoropoulos, P.A., Kalmanti, M., Fostinis, Y., and Gravanis, A. (1996). Altered actin polymerization dynamics in various malignant cell types: evidence for differential sensitivity to cytochalasin B. Biochem. Pharmacol. *52*, 1339–1346. https://doi.org/10.1016/S0006-2952(96)00389-9.

47. Levental, K.R., Yu, H., Kass, L., Lakins, J.N., Egeblad, M., Erler, J.T., Fong, S.F.T., Csiszar, K., Giaccia, A., Weninger, W., et al. (2009). Matrix crosslinking forces tumor progression by enhancing integrin signaling. Cell *139*, 891–906. https://doi.org/10.1016/j.cell.2009.10.027.

48. Chow, T.W., Hellums, J.D., Moake, J.L., and Kroll, M.H. (1992). Shear stress-induced von Willebrand factor binding to platelet glycoprotein Ib initiates calcium influx associated with aggregation. Blood *80*, 113–120.

49. Kamioka, H., Sugawara, Y., Murshid, S.A., Ishihara, Y., Honjo, T., and Takano-Yamamoto, T. (2006). Fluid shear stress induces less calcium response in a single primary osteocyte than in a single osteoblast: implication of different focal adhesion formation. J. Bone Miner. Res. *21*, 1012–1021. https://doi.org/10.1359/jbmr.060408.

50. Yamamoto, K., Korenaga, R., Kamiya, A., and Ando, J. (2000). Fluid shear stress activates Ca2+ influx into human endothelial cells via P2X4 purinoceptors. Circ. Res. *87*, 385–391. https://doi.org/10.1161/01.RES.87.5.385.

51. Yankaskas, C.L., Bera, K., Stoletov, K., Serra, S.A., Carrillo-Garcia, J., Tuntithavornwat, S., Mistriotis, P., Lewis, J.D., Valverde, M.A., and Konstantopoulos, K. (2021). The fluid shear stress sensor TRPM7 regulates tumor cell intravasation. Sci. Adv. *7*, eabh3457. https://doi.org/10.1126/sciadv.abh3457.

52. Choi, H.Y., Yang, G.-M., Dayem, A.A., Saha, S.K., Kim, K., Yoo, Y., Hong, K., Kim, J.-H., Yee, C., Lee, K.-M., and Cho, S.G. (2019). Hydrodynamic shear stress promotes epithelial-mesenchymal transition by downregulating ERK and GSK3β activities. Breast Cancer Res. *21*, 6. https://doi.org/10.1186/s13058-018-1071-2.

53. Gnanasambandam, R., Ghatak, C., Yasmann, A., Nishizawa, K., Sachs, F., Ladokhin, A.S., Sukharev, S.I., and Suchyna, T.M. (2017). GsMTx4: mechanism of inhibiting mechanosensitive ion channels. Biophys. J. *112*, 31–45. https://doi.org/10.1016/j.bpj.2016.11.013.

54. Denisin, A.K., and Pruitt, B.L. (2016). Tuning the range of polyacrylamide gel stiffness for mechanobiology applications. ACS Appl. Mater. Interfaces *8*, 21893–21902. https://doi.org/10.1021/acsami.5b09344.

55. Califano, J.P., and Reinhart-King, C.A. (2008). A balance of substrate mechanics and matrix chemistry regulates endothelial cell network assembly. Cell. Mol. Bioeng. *1*, 122–132. https://doi.org/10.1007/s12195-008-0022-x.

56. Syed, S., Karadaghy, A., and Zustiak, S. (2015). Simple polyacrylamide-based multiwell stiffness assay for the study of stiffness-dependent cell responses. JoVE *97*, 52643. https://doi.org/10.3791/52643.

57. Taufalele, P.V., VanderBurgh, J.A., Muñoz, A., Zanotelli, M.R., and Reinhart-King, C.A. (2019). Fiber alignment drives changes in architectural and mechanical features in collagen matrices. PLoS One *14*, e0216537. https://doi.org/10.1371/journal.pone.0216537.

58. Gallagher, S.R. (2007). One-dimensional SDS gel electrophoresis of proteins. Curr. Protoc. Cell Biol. *97*, 10–12. https://doi.org/10.1002/0471143030.cb0601s37.

STAR★METHODS

KEY RESOURCES TABLE

REAGENT or RESOURCE	SOURCE	IDENTIFIER
Antibodies		
Mouse anti-human vimentin monoclonal antibody	Thermo Fischer Scientific	Cat#: 14-9897-82; RRID: AB_10597910
Rabbit anti-human E-cadherin monoclonal antibody	Cell Signaling Technologies	Cat#: 24E10
GAPDH antibody	EMD Millipore	Cat#: MAB374;ID: RRID: AB_2107445
IRDye 800CW goat anti-rabbit secondary antibody	LICOR	Cat#: 926- 32211
IRDye 800CW goat anti-mouse secondary antibody	LICOR	Cat#: 926-32210
Chemicals, peptides, and recombinant proteins		
RPMI 1640 media 1x	Gibco	Cat#: 11875-093
Fetal bovine serum	Gibco	Cat#: 16140071
Pen/Strep	Gibco	Cat#: 15140-122
0.05% trypsin-EDTA 1x	Gibco	Cat#: 25300-054
Yoda1	Tocris	Cat#: 5586
DMSO	ATCC	Cat#: 4-X-5
GsMTx-4	Abcam	Cat#: ab141871
DPBS with Ca^{2+} and Mg^{2+}	Sigma Life Science	Cat#: D1283-500ML
Polyethyleneimine	Sigma Aldrich	Cat#: 910791
Glutaraldehyde	Sigma Aldrich	Cat#: G7776-10ML
Acrylamide	BIO RAD	Cat#: 1610140
Bis-acrylamide	BIO RAD	Cat#: 1610142
TEMED	Research Products International	Cat#: T18000-0.25
HEPES	Sigma Aldrich	Cat#: H4034-100G
Ammonium persulfate	BIO RAD	Cat#: 1610700
Sulfo-SANPAH	Sigma Aldrich	Cat#: 803332-50MG
Collagen I	Corning	Cat#: 354236
Paraformaldehyde	Electron Microscopy Sciences	Cat#: 15714S
Triton-X-100	Sigma Aldrich	Cat#: 9002-93-1
Bovine serum albumin	Sigma Aldrich	Cat#: A1470-100G
DAPI	Invitrogen	Cat#: D1306
Antifade mounting media	Vectrashield	Cat#: H-1000
4x Laemmli sample buffer	BIO RAD	Cat#: 1610747
c0mplete tablets MINI, EDTA free protease inhibitor cocktail	Sigma Aldrich	Cat#: 4693159001
Trans-Blot Turbo Midi PVDF Transfer Pack	BIO-RAD	Cat#: 1704157
2-mercaptoethanol	Sigma Aldrich	Cat#: M3148-100ML
Lauryl sulfate	Research Products International	Cat#: L22010
Sodium chloride	Research Products International	Cat#: S23020-1000.0
TRIS base	Research Products International	Cat#: T600400-1000.0
Glycine	Research Products International	Cat#: G36050-1000.0
Methanol	Fischer Chemical	Cat#: A465-4
30% acrylamide/bis solution 37.5:1 with 2.6% crosslinker	BIO RAD	Cat#: 1610158
10x Tris/Glycine/SDS running buffer	BIO RAD	Cat#: 1610732
Extra thick blot paper	BIO RAD	Cat#: 1703967
Intercept blocking buffer TBS	LICOR	Cat#: 927-60001

(*Continued on next page*)

Continued

REAGENT or RESOURCE	SOURCE	IDENTIFIER
Critical commercial assays		
Fluo-4	Thermo Fischer Scientific	Cat#: F14201
ActinRed™ 555 ReadyProbes™	Invitrogen	Cat#: R37112
Experimental models: cell lines		
Human: DU145	ATCC	Cat#: HTB-81
Human: PC3	ATCC	Cat#: CRL-1435
Software and algorithms		
GraphPad Prism version 9 for Windows	GraphPad Software	N/A
Image Studio software	LICOR	N/A
Excel	Microsoft	N/A
Other		
22x22mm glass coverslips	Globe Scientific	Cat#: 1401-10
PDC-001 plasma cleaner	Harrick Plasma	N/A
MA6 mask aligner	Karl Suss	N/A
Atomic force microscope	Asylum Research	N/A
Silicon nitride cantilever with a theoretical spring constant of 0.06N/m that had a borosilicate bead of 5μm in diameter attached at the tip	Novascan	N/A
Olympus IX81 inverted microscope	Olympus	N/A
Glass slides	VWR	Cat#: 48311-703
LICOR Odyssey Fc	LICOR	N/A

RESOURCE AVAILABILITY

Lead contact

Further information on resources and reagents should be directed to the lead contact, Dr. Michael R. King (mike.king@vanderbilt.edu).

Materials availability

Materials generated in this study are available from the lead contact, Dr. Michael R. King (mike.king@vanderbilt.edu).

Data and code availability

All data presented in this study will be shared upon reasonable request by the lead contact, Dr. Michael R. King (mike.king@vanderbilt.edu). This paper does not report any original code. Additional information required to reanalyze the data reported in this paper is available from the lead contact upon request.

EXPERIMENTAL MODEL AND SUBJECT DETAILS

Cell culture and reagents

The metastatic prostate cell lines PC3 (CRL-1435, ATCC, Manassas, VA, USA) and DU145 (HTB-81, ATCC, Manassas, VA, USA) were cultured in RPMI 1640 media 1x (11875-093, Gibco, Paisley, UK) supplemented with 10% (v/v) fetal bovine serum (16140071, Gibco, Paisley, UK) and 1% (v/v) PenStrep (15140-122-100ML, Gibco, Grand Island, NY, USA). PC3 cells are considered a highly metastatic cell line in the literature, while DU145 cells are classified as moderately metastatic (Lima et al., 2018). Cells were incubated in humidified conditions at 37℃ and 5% CO_2 and passaged before exceeding 90% confluency. All experiments were performed in 6-well plates and substrates were sterilized under UV light for 45 min prior to cell seeding. Cells were washed in Ca^{2+} and Mg^{2+} free DPBS (21-031-CM, Corning, Manassas, VA, USA), treated with 0.05% trypsin-EDTA 1x (25300-054, Gibco, Grand Island, NY, USA) for 3 to 5 min, and resuspended in supplemented media before centrifugation at 300 xg for 5 min. Cell pellets were resuspended in supplemented media at a concentration of 0.2 x 10^6 cells/mL, and 1mL of the cell suspension was

pipetted into each well. Cells were incubated for a total of 72 hr on the substrates. To study the effect of pharmacologically activating Piezo1, cells were treated with 10μM Yoda1 (5586, Tocris, Minneapolis, MN, USA), and 0.1% (v/v) DMSO (4-X-5, ATCC, Manassas, VA, USA) was used as a vehicle control.[24] To study the effect of pharmacologically inhibiting Piezo1, cells were treated with 2.5μM GsMTx-4 (ab141871, Abcam, Waltham, MA,USA), and 1.25% (v/v) DPBS with Ca^{2+} and Mg^{2+} (D1283-500ML, Sigma Life Science, St. Louis, MO, USA) was used as a vehicle control. Treatments took place at the 24-hr mark during the 72-hr incubation, allowing cells time to adhere to the substrate surface prior to treatment.

Polyacrylamide gel preparation

22x22mm glass coverslips (1401-10, Globe Scientific, Mahwah, NJ, USA) were plasma cleaned with a PDC-001 plasma cleaner (Harrick Plasma, Ithaca, NY, USA) for 2 min and placed in a bath of 1% (v/v) polyethyleneimine (910791,Sigma Aldrich, St. Louis, MO, USA) in Milli-Q filtered water for 10 min. Coverslips were then washed 3 times in Milli-Q filtered water for 5 min and inverted onto a 200 μL drop of a 0.1% (v/v) glutaraldehyde solution (G7776-10ML, Sigma Aldrich, St. Louis, MO, USA) in DPBS with Ca^{2+} and Mg^{2+} for 30 min. The coverslips were washed 3 additional times in Milli-Q filtered water for 5 min and dried overnight. PA gels with Young's modulus of 5kPa and 60kPa were synthesized by varying the concentrations of acrylamide solution relative to bis-acrylamide.[54] Gel precursor solutions were mixed for the 5kPa gel at a ratio of 7.5% (v/v) acrylamide solution (1610140, BIO RAD, Hercules, CA, USA) to 0.175% (v/v) bis-acrylamide solution (1610142, BIO RAD, Hercules, CA, USA),.[55] The 60kPa gel precursor solution was prepared with a ratio of 13.5% (v/v) acrylamide solution to 0.42% (v/v) bis-acrylamide solution. Both precursor solutions also contained 0.05% (v/v) TEMED (T18000-0.25, Research Products International, Mt. Prospect, IL, USA) and 30mM HEPES (H4034-100G, Sigma Aldrich, St. Louis, MO, USA) pH=6, and were adjusted to pH=6. Solutions were degassed for 30 min and then polymerization was initiated by adding 10% (w/v) ammonium persulfate (1610700, BIO RAD, Hercules, CA, USA) in Milli-Q filtered water, to reach a final concentration of 0.1% (w/v) of ammonium persulfate. A 40μL drop of the precursor solution was pipetted onto the activated side of the coverslip and sandwiched with a second 22x22mm coverslip coated in an anti-adherence solution for 1 hr. PA gels were then separated from the second cover slip and washed 3 times in PBS with Ca^{2+} and Mg^{2+}.

For collagen coatings, each gel was inverted onto a 100μL drop of 10mg/mL Sulfo-SANPAH solution (803332-50MG, Sigma Aldrich, St. Louis, MO, USA) in Milli-Q filtered water and cured using a UV flood exposure on a Karl Suss MA6 mask aligner in the Vanderbilt Institute for Nanoscale Science and Engineering (VINSE) cleanroom.[56] After 3 washes in Milli-Q filtered water, gels were incubated on a 400μL drop of 0.1mg/mL collagen I (354236, Corning, Bedford, MA, USA) in HEPES pH=8 on ice for 2 hr. Finally, gels were incubated in 1mL of 1:1000 ethanolamine in PBS with Ca^{2+} and Mg^{2+} for 20 min. Glass coverslips without PA gels adhered to the surface were used as a control, simulating an extremely stiff environment for the cells. These surfaces were activated and then coated with collagen I following the procedure described above.

The PA gel elastic modulus was confirmed via contact mode atomic force microscopy (AFM) (MFP-3D Asylum Research, CA, USA).[57] Measurements were taken at 16 locations in each gel within a 120x120μm grid. Indentations were performed using a silicon nitride cantilever with a theoretical spring constant of 0.06N/m that had a borosilicate bead of 5μm in diameter attached at the tip (Novascan, Boone, IA). Before taking measurements, the AFM tips were calibrated, and the experimental spring constant was measured to be 0.163N/m $\pm$ 0.019N/m. Asylum curve fitting software was used to calculate the gel elastic modulus from the force curves using the Hertz model with a Poisson's ratio of 0.45.

METHOD DETAILS

Calcium imaging

A stock solution of 50μg of Fluo-4 (F14201, Thermo Fischer Scientific, Milton Park, UK) in 50μL of pluronics (AS-84041, Anaspec Inc, Fremont, CA, USA) was prepared, and then diluted down to 2μg/mL in serum-free RPMI 1640 (SFM). Substrates with cells grown for 3 days were transferred to clean 6-well plates with 1mL of Fluo-4 in SFM supplemented with each treatment: 10μM Yoda1, 0.1% (v/v) DMSO, 2.5μM GsMTx-4, and 1.25% (v/v) DPBS with Ca^{2+} and Mg^{2+}. Cells were incubated in the dark at RT for 45 min and then washed with DPBS with Ca^{2+} and Mg^{2+} supplemented with each of the different treatments. Imaging was performed on an Olympus IX81 inverted microscope using a 10x objective and a 510/20 (excitation/emission) filter set. Yoda1-treated cells grown on glass slides were first imaged to set the acquisition parameters. Images was captured at 5 random locations on each substrate.

Image processing and analysis were performed with FIJI using the macro function and calculated using Equation 1. The first step was to identify the cells as regions of interest for mean fluorescence intensity measurement. All images were converted to 8-bit and then made binary via the thresholding tool. The thresholding parameters were set using an image from the Yoda1-treated cells grown on glass. Regions of interest (ROIs) were identified using the particle analyzer tool set to recognize features of 20 to 750μm^2 and stored on the ROI manager. The original image was then reopened, the ROIs overlaid, and the mean fluorescence intensity was calculated for each cell using the following equation:

$$\frac{\Delta F}{F_0} = \frac{F_{average} - F_0}{F_0} \quad \text{(Equation 1)}$$

$F_{average}$ is the average of the mean fluorescence of all the cells for each of the 5 images taken. F_0 is the average fluorescence intensity of the background. This was sampled using the square tool on FIJI in 3 random locations and then averaged for each image. A total of 3 biological replicates was performed and the $\Delta F/F_0$ values for each of the 5 images each were averaged and plotted on GraphPad Prism version 9 for Windows (GraphPad Software, San Diego, California USA). Images were pseudo-colored with the mpl-magma LUT on FIJI.

Cell shape and actin polymerization assay

After incubation and treatments, substrates with cells were placed in a clean 6-well plate. Cells were fixed in 4% (v/v) paraformaldehyde (15714S, Electron Microscopy Sciences, Hatfield, PA, USA) in DPBS for 15 min, and then permeabilized in 1% (v/v) Triton-X-100 (9002-93-1, Sigma Aldrich, Darmstadt, Germany) in DPBS for 10 min. Blocking was carried out for 2 hr in 5% (v/v) bovine serum albumin (BSA) (A1470-100G, Sigma Aldrich, St. Louis, MO, USA) in DPBS and then the cells were stained with an ActinRed™ 555 ReadyProbes™ reagent (R37112, Invitrogen, Eugene, OR, USA) and 1.5:1000 DAPI (D1306, Invitrogen, Eugene, OR, USA) cocktail in 5% (v/v) BSA in DPBS. Coverslips with a drop of antifade mounting media (H-1000, Vectrashield, Burlingame, CA, USA) were mounted onto glass slides (48311-703, VWR, Radnor, PA, USA).

Imaging was performed on an Olympus IX81 inverted microscope using a 20x objective. F-actin was observed using a 605/70 (excitation/emission) filter set and DAPI with a 460/50 (excitation/emission) filter set. 5 images of each treatment condition were captured at random locations around each substrate. A total of 3 biological replicates was performed for each of the treatments on the 3 different substrates. Image processing and analysis was performed on FIJI using the macro function. 10 random nuclei were selected for each image on each blue channel image. The blue channel (DAPI) and red channel (F-actin) were merged into composite images and then the 10 randomly selected cells were manually contoured using the freehand selections tool. ROIs were saved onto the ROI manager on FIJI. Aspect ratio and mean fluorescence were measured for all 10 contoured cells per condition. For F-actin fluorescence, background noise was sampled as described earlier for the calcium image analysis. Equation 1 was used to calculate the $\Delta F/F_0$ value for each cell, where $F_{average}$ represents each individual cell's mean fluorescence and F_0 is the average of the 3 background measurements. All measurements were taken using the FIJI ROI manager measurement tool.

Western blotting

Cells on substrates were rinsed with DPBS and lysed using 4x Laemmli sample buffer (1610747, BIO RAD, Hercules, CA, USA) supplemented with complete tablets MINI, EDTA free protease inhibitor cocktail (4693159001, Sigma Aldrich, St. Louis, MO, USA). Electrophoresis using 10% sodium dodecyl sulfate-polyacrylamide gels was performed, followed by a semi-dry transfer onto a PVDF membrane using the BIO-RAD Trans-Blot Turbo Transfer System (1704157, BIO RAD, Hercules, CA, USA).[58] The materials used for this were: 2-mercaptoethanol (M3148-100ML, Sigma Aldrich, St. Louis, MO, USA), lauryl sulfate (L22010, Research Products International, Mt. Prospect, IL, USA), sodium chloride (S23020-1000.0, Research Products International, Mt. Prospect, IL, USA), TRIS base (T600400-1000.0, Research Products International, Mt. Prospect, IL, USA), glycine (G36050-1000.0, Research Products International, Mt. Prospect, IL, USA), methanol (A465-4, Fischer Chemical, Geel, Belgium), 30% acrylamide/bis solution 37.5:1 with 2.6% cross-linker (1610158, BIO RAD, Hercules, CA, USA), 10x Tris/Glycine/SDS running buffer (1610732, BIO RAD, Hercules, CA, USA), and extra thick blot paper (1703967, BIO RAD, Hercules, CA, USA).

After transfer, PVDF membranes were blocked in Intercept blocking buffer TBS (927-60001, LICOR, Lincoln, NE, USA). Staining was carried out overnight at 4°C on a rocker with mouse anti-human vimentin monoclonal antibody (14-9897-82, Thermo Fischer Scientific, Milton Park, UK) and the rabbit anti-human E-cadherin monoclonal antibody (24E10, Cell Signaling Technologies, Danvers, MA, USA) diluted at a 1:500 ratio in the blocking buffer. GAPDH antibody (MAB374, EMD Millipore, Burlington, MA, USA) was used as a loading control diluted in blocking buffer at a ratio of 1:2000. The secondary antibodies used were IRDye 800CW goat anti-rabbit secondary antibody (926- 32211, LICOR, Lincoln, Nebraska, USA) and IRDye 800CW goat anti-mouse secondary antibody (926-32210, LICOR, Lincoln, Nebraska, USA) at a dilution of 2:15,000. Membranes were imaged with a LICOR Odyssey Fc (LICOR Biosciences, Lincoln, Nebraska, USA) and quantified with Image Studio software (LICOR Biosciences, Lincoln, Nebraska, USA) following the LICOR housekeeping protein normalization protocol. All values for the treatment groups were then normalized to the relative expression in the untreated cells grown on the 5kPa gels of each replicate. EMT score was calculated by dividing the fluorescent intensity of the vimentin band by the fluorescent intensity of the E-cadherin band.

QUANTIFICATION AND STATISTICAL ANALYSIS

All values are presented as mean $\pm$ SD. Data were obtained from three independent experiments, and each experiment tested 3 different stiffness and 5 treatment conditions (total of 15 groups per experiment). In the experiments requiring microscopy, 5 images were acquired per group per experiment. For the F-actin fluorescence and aspect ratio measurements, 10 cells in each group were chosen by randomly selecting nuclei (blue channel) before merging with the red channel to manually contour cells. Here, outliers were identified by using a ROUT's test with Q set to 5% and removed for analysis. Data analysis was performed on GraphPad Prism using unpaired, parametric t-tests where $p<0.05$ was considered statistically significant.